ELSEVIER

A general formulation for a mathematical PEM fuel cell model

J.J. Baschuk, Xianguo Li*

Department of Mechanical Engineering, University of Waterloo, Waterloo, Ont., Canada N2L 3G1

Abstract

A general formulation for a comprehensive fuel cell model, based on the conservation principle is presented. The model formulation includes the electro-chemical reactions, proton migration, and the mass transport of the gaseous reactants and liquid water. Additionally, the model formulation can be applied to all regions of the PEM fuel cell: the bipolar plates, gas flow channels, electrode backing, catalyst, and polymer electrolyte layers.

The model considers the PEM fuel cell to be composed of three phases: reactant gas, liquid water, and solid. These three phases can co-exist within the gas flow channels, electrode backing, catalyst, and polymer electrolyte layers. The conservation of mass, momentum, species, and energy are applied to each phase, with the technique of volume averaging being used to incorporate the interactions between the phases as interfacial source terms. In order to avoid problems arising from phase discontinuities, the gas and liquid phases are considered as a mixture. The momentum interactions between the fluid and solid phases are modeled by the Darcy-Forchheimer term. The electro-oxidation of H_2 and CO, the reduction of O_2, and the heterogeneous oxidation of H_2 and CO are considered in the catalyst layers. Due to the small pore size of the polymer electrolyte layer, the generalized Stefan–Maxwell equations, with the polymer considered as a diffusing species, are used to describe species transport.

One consequence of considering the gas and liquid phases as a mixture is that expressions for the velocity of the individual phases relative to the mixture must be developed. In the gas flow channels, the flow is assumed homogeneous, while the Darcy and Schlögl equations are used to describe liquid water transport in the electrode backing and polymer electrolyte layers. Thus, two sets of equations, one for the mixture and another for the solid phase, can be developed to describe the processes occurring within a PEM fuel cell. These equations are in a conservative form, and can be solved using computational fluid dynamic techniques.
© 2004 Elsevier B.V. All rights reserved.

Keywords: PEM fuel cell; Mathematical modeling; Two-phase flow

1. Introduction

The use of fossil fuel is a major source of air pollution and contributes to global warming. The transportation sector is a major consumer of fossil fuel, thus eliminating or reducing pollution from transportation sources is a major policy objective. Polymer electrolyte membrane (PEM) fuel cells convert the chemical energy of H_2 and O_2 directly into electrical energy, with water and heat as the only by-products. The low operating temperature allows for quick start-up, and the high power density and mechanically robust construction make PEM fuel cells an attractive re-

placement for the internal combustion (I.C.) engine. Currently, PEM fuel cells are not a commercially viable alternative to the I.C. engine; however, a greater understanding of the processes occurring within a PEM fuel cell can aid in commercialization by providing power output and efficiency gains.

Insight on PEM fuel cells can be obtained through mathematical modeling. Mathematical models use fundamental equations to simulate the processes occurring within a PEM fuel cell. Although several processes occur within a PEM fuel cell, three key processes have the greatest impact on PEM fuel cell performance: the electro-chemical reactions in the catalyst layers, proton migration in the polymer electrolyte membrane layer, and mass transport within all regions of the PEM fuel cell. These processes have been addressed by

* Corresponding author. Tel.: +1 519 888 4567; fax: +1 519 888 6197.
E-mail address: x6li@uwaterloo.ca (X. Li).

Nomenclature

a	activity
A	area (m^2)
$\hat{A}_{\mathcal{R}}$	reactive area per volume (m^{-1})
$\boldsymbol{b}$	body force ($N\,m^{-3}$)
b_i^α	ratio of forward to backward reaction rate constant (mole m^{-3} or m^3 mole^{-1})
B^α	Tafel slope (V)
c	concentration (mole m^{-3})
D	diffusion coefficient ($m^2\,s^{-1}$)
$\mathscr{D}$	binary diffusion coefficient ($m^2\,s^{-1}$)
E	cell voltage (V)
F	Forchheimer coefficient
$\mathscr{F}$	Faraday's constant, 9.6485309×10^4 C mole^{-1}
$\boldsymbol{g}$	acceleration due to gravity ($m\,s^{-2}$)
G	Gibbs function ($J\,kg^{-1}$)
h	convective heat transfer coefficient ($W\,m^{-2}\,K^{-1}$)
H	enthalpy ($J\,kg^{-1}$)
I	current (A)
$\boldsymbol{J}$	current density ($A\,m^{-2}$)
J_0	exchange current density ($A\,m^{-2}$)
$\mathcal{J}_k^\alpha$	mass flux of species α due to molecular diffusion ($kg\,m^{-2}\,s^{-1}$)
k_i^α	forward reaction rate constant ($m\,s^{-1}$ or mole $m^{-2}\,s^{-1}$)
k_{rk}	relative permeability of phase k
K	permeability (m^2)
$\mathbb{K}_e$	equilibrium constant for the acid-base reaction in the polymer electrolyte
$\mathscr{L}$	water content of the polymer electrolyte
L_k^Ψ	correction applied to property Ψ for the porous media structure
$\hat{M}$	molecular weight ($kg\,mole^{-1}$)
$\boldsymbol{n}_{kn}$	unit normal of the interface between phases k and n
N	molar flux (mole $m^{-2}\,s^{-1}$)
P	pressure (Pa)
$\dot{\mathscr{P}}^\alpha$	production of species α (mole $m^{-3}\,s^{-1}$)
$P_{sat}^{H_2O}$	vapor pressure of water (Pa)
$\boldsymbol{q}$	heat flux due to conduction and species diffusion, $W\,m^{-2}$
Q_{react}	heat of reaction ($W\,m^{-3}$)
q_{react}	heat of reaction ($W\,m^{-2}$)
r	radius, m; interaction parameter for CO adsorption ($J\,mole^{-1}$)
$\mathcal{R}$	reaction rate (mole $m^{-2}\,s^{-1}$)
$\mathscr{R}$	universal gas constant, $8.31451\,J\,mole^{-1}\,K^{-1}$
s_k	saturation of phase k
S	entropy ($J\,kg^{-1}\,K^{-1}$)
$\mathcal{S}_{energy}$	source term in the conservation of energy equation ($W\,m^{-3}$)
$\mathcal{S}_{mom}$	source term in the conservation of momentum equation ($N\,m^{-3}$)
$\mathcal{S}_{species}$	source term in the conservation of species equation ($kg\,m^{-3}\,s^{-1}$)
t	time (s)
T	temperature (K)
$\boldsymbol{u}$	velocity ($m\,s^{-1}$)
$\boldsymbol{u}_{kn}$	velocity of the interface between phases k and n ($m\,s^{-1}$)
V	volume (m^3)
$\boldsymbol{w}$	relative phase velocity ($m\,s^{-1}$)
$\boldsymbol{W}$	mass flux ($kg\,m^{-2}\,s^{-1}$)
x_k^α	mole fraction of species α
z_α	charge of species α

Greek letters

β	symmetry factor for the CO adsorption/desorption reaction
γ_k^α	activity coefficient of species α
$\Gamma_{E,k}$	interfacial source term for energy conservation ($J\,m^{-3}\,s^{-1}$)
$\Gamma_{F,k}$	interfacial source term for momentum conservation ($N\,m^{-3}\,s^{-1}$)
$\Gamma_{M,k}$	interfacial source term for mass conservation ($kg\,m^{-3}\,s^{-1}$)
$\Gamma_{S,k}^\alpha$	interfacial source term for species conservation ($kg\,m^{-3}\,s^{-1}$)
ϵ_k	volume fraction of phase k
η	overpotential (V)
θ_c	contact angle
θ_s^α	fraction of reaction sites covered by species α
$\kappa_{\alpha,k}$	electrical conductivity ($S\,m^{-1}$)
λ	thermal conductivity ($W\,m^{-1}\,K^{-1}$)
μ	viscosity ($kg\,m^{-1}\,s^{-1}$)
$\hat{\mu}_k^\alpha$	electro-chemical energy of species α ($J\,mole^{-1}$)
ρ	density ($kg\,m^{-3}$)
σ	surface tension ($N\,m^{-1}$)
$\boldsymbol{\tau}_k$	viscous stress ($N\,m^{-2}$)
Φ	potential (V)
ϕ	void fraction
ω_k^α	mass fraction of species α

Subscripts

a	anode
c	cathode; capillary
cell	cell
e	polymer electrolyte
g	gas
i	interface
l	liquid
m	mixture
ref	reference value

rev	reversible
s	solid

Superscripts

a	anode
c	cathode
e	polymer electrolyte
eff	effective value

Overbars

´	per unit volume (m^{-3})
‾	equilibrium value
˘	correction for dispersion
^	molar units

Operators

$\langle\rangle$	total-volume average
$\langle\rangle^*$	phase-volume average

mathematical models in the published literature, with varying degrees of simplifications.

The hydrogen oxidation and oxygen reduction reactions in the catalyst layers were modeled by Bernardi and Verbrugge [1]. The model of Bernardi and Verbrugge [1] assumed that the catalyst layer void regions were filled with polymer electrolyte; other models allow for a void region filled with gas [2] or a combination of gas, liquid and polymer electrolyte [3]. If the hydrogen fuel contains CO, the hydrogen oxidation reaction is inhibited, severely decreasing the efficiency and power output of the PEM fuel cell. This CO-poisoning of the anode was modeled by Wang and Savinell [4], using an empirical correlation for coverage of CO on the anode catalyst surface. Springer et al. [5] addressed CO-poisoning by using detailed reaction kinetics for the adsorption, desorption, and electro-oxidation of hydrogen and carbon monoxide. The most effective method of mitigating CO-poisoning is the introduction of oxygen, with concentrations ranging from 1 to 4%, into the anode fuel stream; this is referred to as O_2-bleeding. The adsorption, desorption, electro-oxidation, and heterogeneous oxidation of CO, hydrogen, and oxygen were incorporated into a PEM fuel cell model by Baschuk and Li [6].

Since the polymer electrolyte is permeable to water, proton migration is strongly coupled with water transport. Verbrugge and Hill [7] developed a mathematical model of the proton and water migration in the pores of a fully humidified polymer electrolyte membrane. However, the protonic conductivity is a function of the membrane hydration; as well, water transport can be driven by water concentration differentials. Therefore, Springer et al. [8] developed a PEM fuel cell model in which the protonic conductivity was a function of membrane hydration. Water transport in the membrane by the mechanisms of electro-osmotic drag and dif-

fusion were also included within the model. However, the model of Springer et al. [8] was one-dimensional, neglected pressure-driven water transport and relied on an empirical correlation for the conductivity of the membrane. Hence, Thampan et al. [9] used the Dusty Gas Model and acid–base equilibrium to formulate a model describing proton conduction and water transport in the polymer electrolyte membrane.

Both gas and liquid phases exist within the PEM fuel cell, and the mass transport within each phase affects PEM fuel cell performance. The gaseous reactants in the PEM fuel cell must travel from the gas flow channels, through the porous electrode backing layer, and into the catalyst layers. Gurau et al. [10] developed a two-dimensional model that incorporated the reactant flow in the gas flow channels, electrode backing layers, and catalyst layers of a PEM fuel cell. The catalyst layer formulation was similar to that of Bernardi and Verbrugge [1], and the polymer electrolyte layer formulation was similar to that of Verbrugge and Hill [7]. Um et al. [11] developed a model similar to that of Gurau et al. [10], but allowed for the simulation of the transient operation of a PEM fuel cell. Siegel et al. [12] also developed a two-dimensional model, but considered the catalyst layer void regions to be composed of gas and polymer electrolyte membrane. Additionally, proton migration and water transport in the polymer electrolyte membrane layer was incorporated through a formulation similar to Springer et al. [8]. Complex gas flow channel designs require a three-dimensional model in order to accurately simulate the mass transport. Thus, the models of Gurau et al. [10] and Um et al. [11] were extended into three dimensions by Zhou and Liu [13] and Um and Wang [14], respectively. Shimpalee et al. [15] used the commercial CFD software FLUENT to model a PEM fuel cell; the catalyst layers and polymer electrolyte membrane were incorporated as boundary conditions. Heat transfer can be significant in a PEM fuel cell, especially for cells operating within a stack; thus Berning et al. [16] incorporated heat transfer into a three-dimensional PEM fuel cell model. The catalyst layers were considered to be surfaces and modeled with boundary conditions.

Water is produced in the cathode catalyst layer as a product of oxygen reduction. Due to the polymer electrolyte membrane hydration requirements, the reactant streams typically enter the PEM fuel cell fully humidified; hence the water produced in the cathode catalyst layer must exit the PEM fuel cell in liquid form. The two-phase flow in the cathode gas flow channel and electrode backing layer was considered by Wang et al. [17]. Using Darcy's law and the Multi-phase Mixture Model (MMM) [18], liquid water transport in the electrode backing layer was expressed as a function of the capillary pressure and gravity. He et al. [19] used a two-fluid analysis to model the liquid water transport in the cathode catalyst layer; the liquid water velocity was assumed to be proportional to the gas velocity and liquid saturation gradient. Shimpalee et al. [20] added liquid water transport to the model of Shimpalee et al. [15] by treating liquid water as a diffusing species.

You and Liu [21] used a mixture formulation, similar to [18], to add liquid water transport to the model of Gurau et al. [10]. Ferng et al. [22] modeled the two-phase flow in the cathode gas flow channel and electrode backing layer by assuming that the gas and liquid phases had the same velocity. The wetting nature of the pores has a significant effect on the capillary pressure, and thus on liquid water transport. Hence, Stockie [23] simulated liquid water transport in the electrode backing layer for both hydrophilic and hydrophobic wettabilities. In addition, the water contact angle within the pores and the porosity also affect the capillary pressure, and, correspondingly, the liquid water transport. Therefore, Pasaogullari and Wang [24,25] modeled liquid water transport in the electrode backing layer for different contact angles, porosities, and wettabilities.

The three key processes in a PEM fuel cell, the electrochemical reactions, proton migration, and mass transport, are strongly coupled. However, the aforementioned models, Refs. [1–25], either utilize a formulation that does not model all three key processes in sufficient detail, or do not incorporate the entire PEM fuel cell within the model. Currently, including all three key processes in a detailed manner is difficult, since no general formulation exists for a PEM fuel cell: governing equations are currently derived for a specific layer or process within the PEM fuel cell. Therefore, the objective of this paper is to present a comprehensive, mathematical model from which other future modeling simulation studies can be carried out.

The physical problem of the PEM fuel cell is discussed, with an emphasis placed on the processes occurring within the cell and the structure and nature of the flow in each layer. The input and output parameters for the model are chosen to correspond with the dependent and independent parameters of a PEM fuel cell experimental investigation. Within the PEM fuel cell, several phases co-exist: gas, liquid, and solid. The interactions between the gas, liquid and solid phases within the PEM fuel cell are included using the technique of volume averaging. The volume-averaged conservation equations apply throughout the PEM fuel cell, with certain terms having unique forms in each layer of the PEM fuel cell. Since the gas and liquid phases can be discontinuous within the PEM fuel cell, a mixture approach is used whereby the gas and liquid are considered as a single, continuous pseudo-fluid, or mixture; conservation equations are then developed for the pseudo-fluid.

2. Physical problem

A PEM fuel cell consists of several components, and several processes occur within each component, as illustrated in Fig. 1. The reactant gas streams enter the fuel cell through the gas flow channels, which are grooved into the bipolar plates. For a single PEM fuel cell, the bipolar plates are also referred to as flow distribution plates. The bipolar plates are typically made of graphite; the gas flow channels are ap-
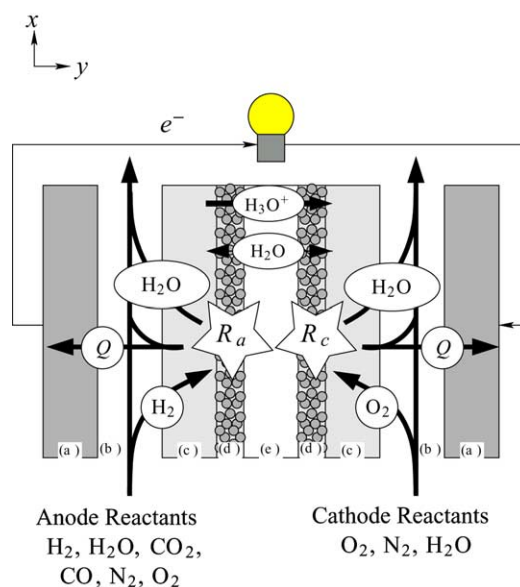

Fig. 1. The processes occurring within a PEM fuel cell. The PEM fuel cell is composed of the (a) bipolar plate, (b) gas flow channel, (c) electrode backing layer, (d) catalyst layer, and (e) polymer electrolyte layer.

proximately 1 mm thick, while the entire bipolar plate has a thickness of approximately 2 mm [26]. The main reactant on the anode side of the PEM fuel cell is hydrogen. However, if the hydrogen is formed from a hydrocarbon source, carbon dioxide and carbon monoxide can also be present. The presence of carbon monoxide, in concentrations of greater than 2 ppm, inhibits the oxidation of hydrogen in the anode catalyst layer (CO-poisoning) [27]. Introducing oxygen, in concentrations of 1–4%, into the anode gas stream can mitigate CO-poisoning (O_2-bleeding [28]); hence oxygen and nitrogen can be present in the anode gas flow channels. Oxygen is the reactant on the cathode side of the cell, and nitrogen can be present if air is used as the oxidant. The polymer electrolyte requires humidification; hence both the anode and cathode streams are generally fully humidified.

In order to reach the catalyst layers, the reactants must pass through the porous, electrode backing layers. Constructed of carbon paper or cloth, the electrode backing layers are approximately 200 μm in thickness [26]. The electrode backing layers also allow liquid water to exit the catalyst layers and enter the gas flow channels.

The conversion of the chemical energy of the reactants into electrical energy, heat, and liquid water occurs in the catalyst layers, which have a thickness of approximately 5 μm [26]. The catalyst layers are also porous; reactant gas, liquid water, and polymer electrolyte occupy the void space and the solid matrix consists of carbon-supported platinum catalyst. If the fuel is CO-free, the overall reaction (R_a) in the anode catalyst layer is hydrogen oxidation:

$$H_2 \longrightarrow 2H^+ + 2e^-. \tag{1}$$

The polymer electrolyte is electronically insulative; hence the electron produced by the above hydrogen oxidation must pass

through the electrode backing layer, bipolar plate, and the external load. The proton in reaction (1) is transferred through the polymer electrolyte and participates in the reduction of oxygen in the cathode catalyst layer:

$$2H^+ + 2e^- + \frac{1}{2}O_2 \longrightarrow H_2O_{(l)}. \tag{2}$$
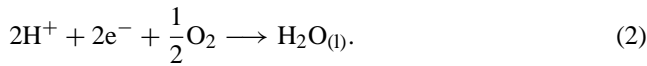
The combination of reactions (1) and (2) is the overall PEM fuel cell reaction:

$$H_2 + \frac{1}{2}O_2 \longrightarrow H_2O_{(l)} + heat + electrical\ energy. \tag{3}$$
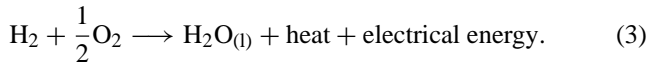
The heat produced by the electro-chemical reactions must exit the PEM fuel cell. The heat can be transported through conduction in the solid phase of the electrode backing layers and bipolar plates, or through convection and conduction in the fluid phases.

The polymer electrolyte layer consists of a sulfonated fluoropolymer, which is similar to Teflon. The fluorinated carbon chains terminate in SO_3H groups, which when in contact with water, dissociate into SO_3^- and H_3O^+ ions. The presence of the hydronium ions allow the sulfonated fluoropolymer to act as an electrolyte; the protons produced in the anode catalyst layer can be conducted through the membrane in order to react in the cathode catalyst layer. The electrolyte is permeable to reactant gases and water, although the permeability to reactant gases is low and reactant cross-over is small. The protonic conductivity of the membrane decreases if the water content of the membrane is low; hence, external humidification from the reactant streams is necessary in order to prevent electrolyte dehydration. The thickness of the polymer electrolyte layer ranges from 50 to 250 μm [29] and the most popular polymer electrolyte employed for PEM fuel cells is Nafion.

Each layer of the PEM fuel cell has a unique structure, as shown in Fig. 2. The anode and cathode reactants typically enter the gas flow channels fully humidified. As a result, the water produced by the PEM fuel cell must be entrained within the gas flow channels as small liquid droplets. Two-phase, porous media flow occurs within the electrode backing layers, with the liquid water being driven by capillary pressure. The electrode backing layer is manufactured such that there is a mix of hydrophobic and hydrophilic pores.

The transport of water, protons, and reactant gas in the polymer electrolyte can be explained by the ionic cluster model of Gierke and Hsu [30]. In the presence of water, the Nafion membrane is composed of three regions [31]. Liquid water and hydronium ions are contained within clusters that have a diameter of approximately 4 nm [30]. Channels interconnect the clusters, with the channels having a diameter of approximately 1 nm [30]. Both the channels and the clusters are lined with immobile sulfonate ions. Between the clusters and the rigid, hydrophobic backbone of the polymer, exists the amorphous part of the perfluorinated backbone. This hydrophobic region is permeable to gases, thus transport of reactant gas occurs in this region.

The flow characteristics in the catalyst layer are a combination of the flow in the electrode backing layers and polymer electrolyte layer. Two-phase, porous media flow occurs in the electrolyte-free void space, while liquid water and reactant gas are also transported within the electrolyte. Electrochemical reactions occur at the catalyst/electrolyte interface, thus the reactant gases are consumed and, in the cathode catalyst layer, liquid water is produced.

3. Model input and output

The input and output parameters of the PEM fuel cell model are chosen with regard to an experimental investigation into PEM fuel cell performance. The performance of a PEM fuel cell can be characterized by a voltage versus current plot. When testing a PEM fuel cell, several operating conditions can be altered, such as
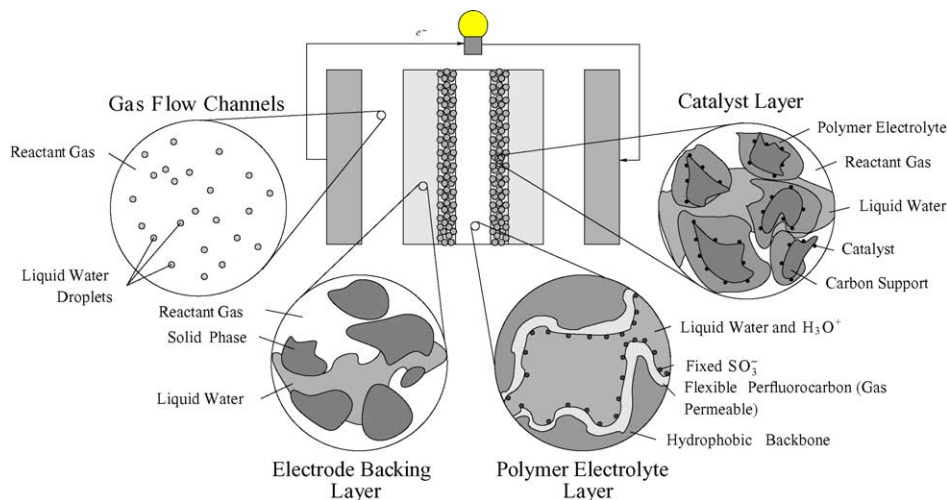

Fig. 2. The nature of the flow in the layers of a PEM fuel cell.

- the inlet concentration, temperature, and flow rate of the reactants;
- the cell temperature;
- the electrical load; and
- either the inlet or outlet pressure.

The temperature variation within the fuel cell is small. Therefore, during operation, the temperature is measured at one location within the cell and referred to as the cell temperature. This cell temperature is controlled by heating or cooling the external surfaces of the PEM fuel cell. The electrical load on the PEM fuel cell is specified by setting the voltage of the PEM fuel cell or the current drawn from the cell. The inlet and outlet pressures are related through the pressure drop in the gas flow channels; hence, specifying both pressures as input conditions is redundant. If the PEM fuel cell is not pressurized, then the gas flow channels exhaust to the atmosphere; thus the outlet pressure is specified. During pressurized operation, the inlet pressure is generally specified and regulated with a back-pressure control valve that is located at the outlet of the gas flow channels.

Therefore, one set of input parameters are the operating conditions, and these become the external boundary conditions for the PEM fuel cell model. The location of the external boundary, for a two-dimensional geometry, is shown as the dark, solid line in Fig. 3. The PEM fuel cell in Fig. 3 has a thickness of Y_L and a height of X_L. The interfaces between the various layers of the PEM fuel cell are also shown in the figure. The bipolar plate/gas flow channel, gas flow channel/electrode backing layer, electrode backing layer/catalyst layer, and catalyst layer/polymer electrolyte layer interfaces in the anode side of the PEM fuel cell are denoted by $Y_{bp/fc}^a$, $Y_{fc/eb}^a$, $Y_{eb/cl}^a$, and $Y_{cl/e}^a$, respectively. Similar notation is used to denote the interfaces on the cathode side, except that the superscript "a" is replaced by "c".

The external boundary conditions can be classified into three groups: the x surfaces excluding the gas flow channels (i.e., $0 \le y \le Y_{bp/fc}^a$, $Y_{fc/eb}^a \le y \le Y_{fc/eb}^c$, and $Y_{bp/fc}^c \le y \le Y_L$); the y surfaces; and the x surfaces of the gas flow chan-
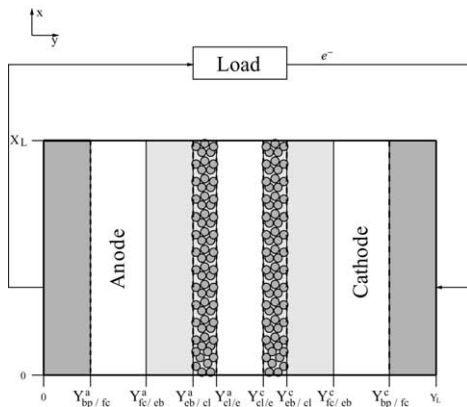

Fig. 3. The boundaries where the boundary conditions for the PEM fuel cell model are imposed. The dark solid line denotes the external boundary, while the dashed line is the location of the internal boundary.

nels (i.e., $Y_{bp/fc}^a < y < Y_{fc/eb}^a$ and $Y_{fc/eb}^c < y < Y_{bp/fc}^c$). The x surfaces, excluding the gas flow channels, are considered as solid, insulated walls. Therefore, the velocity, heat transfer, and species flux are zero:

$$\left\{ \begin{array}{l} \boldsymbol{u}_k = 0 \\ \mathcal{J}_k^\alpha \cdot \hat{\boldsymbol{\imath}} = 0 \\ \boldsymbol{J}_s \cdot \hat{\boldsymbol{\imath}} = 0 \\ \boldsymbol{q}_k \cdot \hat{\boldsymbol{\imath}} = 0, \end{array} \right\} \quad \text{for} \quad \left\{ \begin{array}{l} 0 \le y \le Y_{bp/fc}^a \\ Y_{fc/eb}^a \le y \le Y_{fc/eb}^c \\ Y_{bp/fc}^c \le y \le Y_L \\ x = 0, X_L \end{array} \right\}$$

where $\boldsymbol{u}_k$ is the velocity of phase k, $\mathcal{J}_k^\alpha$ the diffusive flux of species α in phase k, $\boldsymbol{J}_s$ the current density in the solid phase, and $\boldsymbol{q}_k$ the heat flux due to conduction and species diffusion. The unit vector in the x-direction is expressed as $\hat{\boldsymbol{\imath}}$. The boundary condition on the heat flux is an approximation, since the x surfaces of a single PEM fuel cell are generally exposed to the ambient environment. However, the aspect ratio of the cell, Y_L / X_L, is generally much less than 1. Additionally, the temperature of a single PEM fuel cell is controlled by heating or cooling the y surface of the bipolar plate. Therefore, the heat lost or gained from the x surfaces can be considered negligible, compared to the heat transfer at the y surfaces of the bipolar plates.

Since the y surfaces are heated or cooled, boundary conditions on the heat flux must be specified. The heat transfer at the bipolar plates can be specified as either a fixed surface temperature, a specified heat flux, or a convective heat transfer condition:

$$\left\{ \begin{array}{c} T_s = \text{specified} \\ \boldsymbol{q}_s = \text{specified} \\ \boldsymbol{q}_s \cdot \hat{\boldsymbol{\jmath}} \pm h(T_s - T_\infty) = 0 \end{array} \right\} \quad \text{for} \quad \left\{ \begin{array}{l} 0 \le x \le X_L \\ y = 0, Y_L \end{array} \right\}$$

where T_∞ is the ambient air temperature, $\hat{\boldsymbol{\jmath}}$ the unit vector in the y direction, and h the convective heat transfer coefficient.

The cell voltage can be expressed as

$$E = E_{rev} - \eta_{cell}, \tag{4}$$

where E_{rev} is the reversible cell potential and η_{cell} the cell voltage loss, or overpotential. The cell overpotential includes the activation overpotential associated with the electro-chemical reactions, the concentration overpotential caused by mass transport, and the ohmic losses incurred by electron and proton transport within the PEM fuel cell. The reversible cell potential can be found by assuming that the overall fuel cell reaction is in equilibrium:

$$\begin{aligned} E_{rev} &= \frac{\Delta \hat{G}}{2\mathscr{F}} - \frac{\Delta \hat{S}}{2\mathscr{F}}(T - T_{ref}) \\ &\quad + \frac{\mathscr{R}T}{2\mathscr{F}} \ln \left[\left(\frac{P_{H_2}}{P_{ref}} \right) \left(\frac{P_{O_2}}{P_{ref}} \right)^{1/2} \right], \end{aligned} \tag{5}$$

where $\Delta \hat{G}$ is the change in Gibbs energy and $\Delta \hat{S}$ the change in entropy for the overall fuel cell reaction. The inlet temperature and pressure of the reactants are denoted by T and

P, respectively; the universal gas constant and the Faraday constant are given as $\mathscr{R}$ and $\mathscr{F}$, respectively. The subscript "ref" denotes a reference value. Using the standard values for $\Delta\hat{G}$ and $\Delta\hat{S}$, the reversible cell potential can be calculated as

$$E_r = 1.229 - 0.85 \times 10^{-3}(T - 298.15)$$
$$+ 4.31 \times 10^{-5}T \ln[(\bar{P}_{H_2})(\bar{P}_{O_2})^{1/2}],$$

where T is in K and P is in atmospheres.

The absolute value of the potential in the solid phase is arbitrary, and depends on the choice of reference electrode [32]. In this model, the reference electrode is chosen to consist of the solid phase at the open circuit conditions. Therefore, the difference between the potentials on the anode and cathode bipolar plates becomes the cell overpotential [33]. Assuming that the potential on the surface of the bipolar plates is constant, the boundary conditions for the cell potential are

$$\Phi_s|_{y=0} = \eta_{cell}, \qquad \Phi_s|_{y=Y_L} = 0, \qquad (6)$$

where cathode potential, $\Phi_s|_{y=Y_L}$, is arbitrarily defined as zero. Hence, in the PEM fuel cell mathematical model, the cell voltage is calculated by specifying the overpotential. In this approach, the electric double layers in the electrolyte near the two catalyst layers have been neglected. The double layers provide the driving potential needed for proton transport through the electrolyte, but do not contribute to the overall overpotential.

The anode and cathode gas flow channels each have one inlet and one outlet. The inlets can be either on the same side, which is referred to as a co-flow arrangement, or on opposite sides, which is referred to as a counter-flow arrangement. At the inlet, the velocity, species mass fractions, temperatures, and volume fractions are specified for the gas and liquid phases:

$$\left\{ \begin{array}{c} \boldsymbol{u}_k \\ \omega_k^\alpha \\ T_k \\ \epsilon_k \end{array} \right\} = \text{specified} \qquad \text{for} \qquad \left\{ \begin{array}{c} \text{the inlet} \\ Y_{bp/fc}^a < y < Y_{fc/eb}^a \\ Y_{fc/eb}^c < y < Y_{bp/fc}^c \end{array} \right\},$$

where ϵ_k is the volume fraction and the mass fraction of species α within phase k is denoted by ω_k^α.

As mentioned previously, the pressure can be specified at either the inlet or the outlet; here, it is assumed that the cell exhausts to the atmosphere and the pressure is specified at the outlet. The profiles of velocity, mass fraction, and temperature are not known at the outlet; however, if the gas flow channels are extended beyond the PEM fuel cell, the flow becomes fully developed. Thus, the outlet boundary conditions can be expressed as

$$\left\{ \begin{array}{c} P = \text{specified} \\ \frac{\partial}{\partial x}|_{x=X_L+X_\infty} = 0 \end{array} \right\} \qquad \text{for} \qquad \left\{ \begin{array}{c} \text{the outlet} \\ Y_{bp/fc}^a < y < Y_{fc/eb}^a \\ Y_{fc/eb}^c < y < Y_{bp/fc}^c \end{array} \right\},$$

where X_∞ is the extension of the gas flow channels that results in fully developed flow.

The external boundary conditions coincide with the operating conditions of a PEM fuel cell. However, internal boundary conditions, shown as the dashed line in Fig. 3, are also required, due to phase discontinuities. The H_3O^+ ions are only present in the polymer electrolyte and catalyst layers; hence a no-flux boundary condition must be applied at the electrode backing/catalyst layer interfaces:

$$\boldsymbol{W}_e^{H_3O^+} \cdot \hat{\boldsymbol{j}} = 0 \quad \text{for} \quad y = Y_{eb/cl}^a \text{ and } Y_{eb/cl}^c,$$

where $\boldsymbol{W}_e^{H_3O^+}$ is the mass flux of hydronium ions. Likewise, electrons cannot be transported in the polymer electrolyte layer; hence a no-flux boundary condition is also necessary at the catalyst layer/polymer electrolyte membrane layer interfaces:

$$\boldsymbol{J}_s \cdot \hat{\boldsymbol{j}} = 0 \quad \text{for} \quad y = Y_{cl/e}^a \text{ and } Y_{cl/e}^c.$$

Since the bipolar plate is impermeable, the fluid phases disappear at the bipolar plate/gas flow channel interface. Therefore, the appropriate boundary conditions are the no-slip and no-temperature jump conditions:

$$\left\{ \begin{array}{c} \boldsymbol{u}_k = 0 \\ T_g = T_l = T_s \end{array} \right\} \qquad \text{for} \qquad y = Y_{bp/fc}^a \text{ and } Y_{bp/fc}^c.$$

The performance can also be influenced by the manufacture of the PEM fuel cell; this effect is included within the model by input parameters that are referred to as design parameters. These include such parameters as the overall dimensions of the PEM fuel cell and the thickness of each layer. The choice of materials for the bipolar plates influences the heat transfer and electrical conductivity properties of the cell. For the porous electrode backing layer, the porosity and permeability are important input parameters, as well as the nature of the pores: the degree of hydrophobic and hydrophilic behavior influences the capillary pressure. The fraction of the void space occupied by polymer electrolyte in the catalyst layer is also an important design parameter. In addition to the design parameters, the model requires values for the physical properties of the reactant gas and liquid water, such as density, viscosity, diffusivity, and thermal conductivity.

The mathematical model analyzes the transport of mass, momentum, species, and energy within the gas, liquid, and solid phases of the PEM fuel cell. Therefore, the velocity, pressure, concentration, potential, and temperature profiles within the PEM fuel cell are the model output parameters. From these profiles, the mass flux of each species and the current density can be determined. This information is significant because, due to the small geometry and operating environment, direct in situ measurement of these quantities within a PEM fuel cell is difficult, if not impossible. Since the cell voltage is an input parameter, the current output of

the PEM fuel cell is determined with

$$I = \int_{A_{\text{bp}}} \boldsymbol{J}_{\text{s}} \cdot \hat{\boldsymbol{\jmath}} \, \mathrm{d}A, \tag{7}$$

where A_{bp} is the surface area of the bipolar plate and $\boldsymbol{J}_{\text{s}}$ the current density, which changes over the active cell surface.

Therefore, the mathematical model has two inputs: the operating conditions and the design parameters. The operating conditions correspond to the independent variables during the experimental investigation of a PEM fuel cell. The design parameters depend on the manufacture of the PEM fuel cell. Profiles of velocity, pressure, concentration, potential, and temperature are determined by the model as output parameters. Since the cell voltage is specified as an input parameter, the performance of the PEM fuel cell is quantified by the corresponding cell current, or current density distribution.

4. Formulation

Three phases co-exist within the PEM fuel cell: gas, liquid, and solid. The conservation of mass, momentum, species, and energy within the phases are expressed with [34]

$$\frac{\partial \rho_k}{\partial t} + \nabla \cdot (\rho_k \boldsymbol{u}_k) = 0, \tag{8}$$

$$\frac{\partial}{\partial t}(\rho_k \boldsymbol{u}_k) + \nabla \cdot (\rho_k \boldsymbol{u}_k \boldsymbol{u}_k) + \nabla P_k - \nabla \cdot \boldsymbol{\tau}_k - \rho_k \boldsymbol{g} - \boldsymbol{b} = 0, \tag{9}$$

$$\frac{\partial}{\partial t}(\rho_k \omega_k^\alpha) + \nabla \cdot (\rho_k \omega_k^\alpha \boldsymbol{u}_k + \mathcal{J}_k^\alpha) = 0, \tag{10}$$

$$\frac{\partial}{\partial t}(\rho_k H_k) + \nabla \cdot (\rho_k H_k \boldsymbol{u}_k) = -\nabla \cdot \boldsymbol{q}_k + E_k^{\alpha\pm}, \tag{11}$$

where Eqs. (8)–(11) are the conservation equations for mass, momentum, species, and energy, respectively. The subscript k denotes the phase, with $k = g, l$ and s representing the gas, liquid, and solid phases, respectively. Although Eqs. (8)–(11) apply to all three phases, the immobility of the solid phase results in only the conservation of species and energy being relevant to the solid phase.

The density and velocity of the phase are denoted by ρ_k and $\boldsymbol{u}_k$, respectively. In the conservation of momentum, Eq. (9), momentum change due to pressure (P_k), viscous stress ($\boldsymbol{\tau}_k$), gravity ($\boldsymbol{g}$), and a body force ($\boldsymbol{b}$) are included. It is assumed that no reactions take place within either the gas or liquid phases; thus, the conservation of species α within phase k is represented by Eq. (10). The mass fraction of species α within phase k is denoted by ω_k^α, while $\mathcal{J}_k^\alpha$ represents the mass flux of species α due to molecular diffusion. Energy transfer due to pressure work and viscous dissipation are both neglected in the conservation of energy, which is expressed as Eq. (11). The enthalpy of phase k is denoted by H_k, and $\boldsymbol{q}_k$ represents the transport of energy due to conduction and

species diffusion. The enthalpy of the phase does not include any contribution from charged species; hence

$$H_k = \sum_{\alpha \neq \alpha^\pm} \omega_k^\alpha H_k^\alpha, \tag{12}$$

where H_k^α is the enthalpy of species α in phase k and $\alpha^\pm$ represents a charged species. If the polymer electrolyte is free of contaminants, then the only charged species are the H_3O^+ ions in the liquid phase of the polymer electrolyte. The energy of a charged species is potential-dependent; therefore, it is represented by the $E_k^{\alpha^\pm}$ term in the conservation of energy equation:

$$E_k^{\alpha^\pm} = -\boldsymbol{W}_k^{\alpha^\pm} \cdot \nabla H_k^{\alpha^\pm}. \tag{13}$$

Using the Gibbs equation, the enthalpy of a charged species can be expressed in terms of the electro-chemical energy ($\hat{\mu}_k^{\alpha^\pm}$) and the partial molar entropy ($\hat{S}_k^{\alpha^\pm}$) [32]:

$$\hat{H}_k^{\alpha^\pm} = \hat{\mu}_k^{\alpha^\pm} + T_k \hat{S}_k^{\alpha^\pm} \tag{14}$$

The electro-chemical energy can be expressed as

$$\nabla \hat{\mu}_k^{\alpha^\pm} = \mathscr{R} T_k \nabla \ln a_k^{\alpha^\pm} + z_{\alpha^\pm} \mathscr{F} \nabla \Phi_k, \tag{15}$$

where $z_{\alpha^\pm}$ is the charge and $a_k^{\alpha^\pm}$ is the activity [35]:

$$a_k^\alpha = \gamma_k^\alpha x_k^\alpha. \tag{16}$$

The activity coefficient is γ_k^α and x_k^α is the mole fraction. The definition of activity given in Eq. (16) is valid for both charged and uncharged species and for an ideal gas or a dilute solution, the activity coefficient is unity. Therefore, the energy of the charged species can be expressed as

$$E_k^{\alpha^\pm} = -\frac{\boldsymbol{W}_k^{\alpha^\pm}}{\hat{M}_\alpha} \cdot [\mathscr{R} T_k \nabla \ln a_k^{\alpha^\pm} + z_{\alpha^\pm} \mathscr{F} \nabla \Phi_k + \nabla(T_k \hat{S}_k^{\alpha^\pm})]. \tag{17}$$

For the solid phase, the charged species are electrons and only the potential gradient term is relevant; thus Eq. (17) represents Joule heating in the solid phase.

The viscous stress, diffusional mass flux, and the heat flux due to conduction and species diffusion are expressed as [34]

$$\tau_k = \mu_k[\nabla \boldsymbol{u}_k + (\nabla \boldsymbol{u}_k)^\dagger], \tag{18}$$

$$-c_k^\alpha \nabla \ln a_k^\alpha - \frac{z_\alpha c_k^\alpha \mathscr{F}}{} \mathscr{R} T_k \nabla \Phi_k$$

$$= \sum_{\beta \neq \alpha} \frac{\hat{M}_k}{\hat{M}_\alpha \hat{M}_\beta \mathscr{D}_{\alpha-\beta,k}} (\omega_k^\beta \mathcal{J}_k^\alpha - \omega_k^\alpha \mathcal{J}_k^\beta), \tag{19}$$

$$\boldsymbol{q}_k = -\lambda_k \nabla T_k + \sum_\alpha H_k^\alpha \mathcal{J}_k^\alpha. \tag{20}$$

In the expression for viscous stress, † represents the transpose and μ_k is the viscosity of phase k; it is assumed that each phase is a Newtonian fluid and that the dilation effect on the viscous

stress tensor is negligible. The Generalized Stefan–Maxwell equations are used to describe the diffusive mass flux, with the temperature and pressure effects neglected. Since electrons are the only mobile species in the solid phase, the generalized Stefan–Maxwell equation reduces to Ohm's law in the solid phase. The molar concentration is c_k^α and the molecular weights of the phase and species are denoted by $\hat{M}_k$ and $\hat{M}_\alpha$, respectively. In Eq. (20), λ_k is the thermal conductivity.

The transfer of mass, momentum, species, and energy from adjacent phases is absent from the conservation equations presented in Eqs. (8)–(11). In order to account for these processes, the conservation equations must be integrated over a representative volume:

$$\langle \text{conservation equation} \rangle$$

$$= \frac{1}{V_r} \int_{V_r} (\text{conservation equation}) \, dV, \tag{21}$$

where V_r is the representative volume. Using the transport and averaging theorems [36], the volume-averaged conservation equations can be expressed in terms of volume-averaged quantities, such as density and velocity, and interfacial source terms. For quantities such as density and velocity, the phase-volume, or intrinsic, average is defined as

$$\langle \Psi_k \rangle^* = \frac{1}{V_k} \int_{V_k} \Psi_k \, dV, \tag{22}$$

where V_k is the volume of phase k within the representative volume and Ψ_k is a quantity within phase k, such as density or velocity. The phase-volume average of Eq. (22) and the total-volume average of Eq. (21) are related with

$$\frac{\langle \Psi_k \rangle}{\langle \Psi_k \rangle^*} = \frac{V_k}{V_r} = \epsilon_k, \tag{23}$$

where ϵ_k is the volume fraction of phase k within the representative volume.

The general, volume-averaging procedure for two-phase, gas/liquid flows is described by Ishii [37], while Slattery [38] presents the volume-averaging procedure for porous media flows. Additionally, volume-averaging is applied to the modeling of batteries and the porous region of a PEM fuel cell by Wang et al. [39]. After the volume-averaging procedure, the conservation equations become

$$\frac{\partial}{\partial t}(\epsilon_k \langle \rho_k \rangle^*) + \nabla \cdot (\epsilon_k \langle \rho_k \rangle^* \langle \boldsymbol{u}_k \rangle^*) = \Gamma_{M,k}, \tag{24}$$

$$\frac{\partial}{\partial t}(\epsilon_k \langle \rho_k \rangle^* \langle \boldsymbol{u}_k \rangle^*) + \nabla \cdot (\epsilon_k \langle \rho_k \rangle^* \langle \boldsymbol{u}_k \rangle^* \langle \boldsymbol{u}_k \rangle^*)$$
$$+ \nabla(\epsilon_k \langle P_k \rangle^*) - \langle P_k \rangle^* \nabla(\epsilon_k) - \nabla \cdot (\epsilon_k \langle \boldsymbol{\tau}_k \rangle^*)$$
$$- \epsilon_k \langle \rho_k \rangle^* \boldsymbol{g} - \epsilon_k \langle \boldsymbol{b} \rangle^* = \Gamma_{F,k}, \tag{25}$$

$$\frac{\partial}{\partial t}(\epsilon_k \langle \rho_k \rangle^* \langle \omega_k^\alpha \rangle^*) + \nabla \cdot (\epsilon_k \langle \rho_k \rangle^* \langle \omega_k^\alpha \rangle^* \langle \boldsymbol{u}_k \rangle^*$$
$$+ \epsilon_k \langle \mathcal{J}_k^\alpha \rangle^*) = \Gamma_{S,k}^\alpha, \tag{26}$$

$$\frac{\partial}{\partial t}(\epsilon_k \langle \rho_k \rangle^* \langle H_k \rangle^*) + \nabla \cdot (\epsilon_k \langle \rho_k \rangle^* \langle H_k \rangle^* \langle \boldsymbol{u}_k \rangle^*)$$
$$= -\nabla \cdot (\epsilon_k \langle \boldsymbol{q}_k \rangle^*) + \epsilon_k \langle E_k^{\alpha\pm} \rangle^* + \Gamma_{E,k}, \tag{27}$$

where Γ represents the interfacial source terms. The volume-averaged form of the energy of the charged species, $\langle E_k^{\alpha\pm} \rangle^*$, is assumed to be the same as Eq. (17), except that the bulk values are replaced by volume-averaged values. The volume-averaged forms of the viscous stress tensor ($\langle \tau_k \rangle^*$) and heat flux ($\langle q \rangle_k^*$) are

$$\langle \tau_k \rangle^* = \mu_k^{\text{eff}}[\nabla \langle \boldsymbol{u}_k \rangle^* + (\nabla \langle \boldsymbol{u}_k \rangle^*)^\dagger], \tag{28}$$

$$\langle q \rangle_k^* = -\lambda_k^{\text{eff}} \nabla \langle T_k \rangle^* + \sum_\alpha \langle H_k^\alpha \rangle^* \langle \mathcal{J}_k^\alpha \rangle^*, \tag{29}$$

where the effective viscosity and thermal conductivity are denoted by μ_k^{eff} and λ_s^{eff}, respectively. The effective values of viscosity and thermal conductivity depend on the nature of the multiphase flow; however, they have the general form of [40]

$$\Psi_k^{\text{eff}} = (1 + L_k^\Psi)\Psi_k + \breve{\Psi}_k, \tag{30}$$

where L_k^Ψ is the correction for the porous media structure and $\breve{\Psi}_k$ the correction for dispersion and hydrodynamic effects.

Because of the small pore diameters, especially within the polymer electrolyte, molecular interactions between species in the fluid phases and the solid phase can be significant. These interactions can be incorporated within the diffusional mass flux term by considering the solid phase as a diffusing species with a velocity of zero [41]. Thus, the volume-averaged form of the generalized Stefan–Maxwell equations become

$$-\langle c_k^\alpha \rangle^* \nabla \ln \langle a_k^\alpha \rangle^* - \frac{z_\alpha \langle c_k^\alpha \rangle^* \mathscr{F}}{\mathscr{R} \langle T_k \rangle^*} \nabla \langle \Phi_e \rangle^*$$
$$= \sum_{\beta \neq \alpha} \frac{\hat{M}_k}{\hat{M}_\alpha \hat{M}_\beta D_{\alpha-\beta,k}^{\text{eff}}}(\langle \omega_k^\beta \rangle^* \langle \boldsymbol{W}_k^\alpha \rangle^* - \langle \omega_k^\alpha \rangle^* \langle \boldsymbol{W}_k^\beta \rangle^*)$$
$$+ \frac{\langle \boldsymbol{W}_k^\alpha \rangle^*}{\hat{M}_\alpha D_{\alpha-s,k}^{\text{eff}}}, \tag{31}$$

where $\boldsymbol{W}_k^\alpha$ is the total mass flux of species α and $D_{\alpha-s,k}^{\text{eff}}$ represents the interactions between the solid phase and the species within the fluid phases. In regions of the PEM fuel cell where the solid phase does not exist, or does not have an appreciable effect on species mass flux, $D_{\alpha-s,k}^{\text{eff}} \to \infty$ and Eq. (31) reduces to the standard Stefan–Maxwell equation: Eq. (19). An equation for the diffusive mass flux can be obtained by inverting Eq. (31):

$$\langle \mathcal{J}_k^\alpha \rangle^* = -\langle \rho_k \rangle^* \Upsilon_k^\alpha D_{\alpha,k}^{\text{eff}} \nabla \langle \omega_k^\alpha \rangle^* - \frac{\hat{M}_\alpha \kappa_{\alpha,k}^{\text{eff}}}{z_\alpha \mathscr{F}} \nabla \langle \Phi_e \rangle^*$$
$$+ \frac{\langle \omega_k^\alpha \rangle^* D_{\alpha,k}^{\text{eff}}}{(1 - \langle x_k^\alpha \rangle^*)} \sum_{\beta \neq \alpha} \left[\frac{\langle \rho_k \rangle^* \Upsilon_k^\alpha \hat{M}_k \nabla \langle \omega_k^\beta \rangle^*}{\hat{M}_\beta} \right.$$

$$+ \frac{\hat{M}_k \langle \mathcal{J}_k^\beta \rangle^*}{\hat{M}_\beta D_{\alpha-\beta,k}^{\text{eff}}} \Bigg] + \langle \omega_k^\alpha \rangle^* \langle \rho_k \rangle^* \langle \boldsymbol{u}_k \rangle^*$$

$$\times \left[\frac{D_{\alpha,k}^{\text{eff}}}{(1 - \langle x_k^\alpha \rangle^*)} \sum_{\beta \neq \alpha} \frac{\langle x_k^\beta \rangle^*}{D_{\alpha-\beta,k}^{\text{eff}}} - 1 \right], \tag{32}$$

where $D_{\alpha,k}^{\text{eff}}$ is the overall diffusion coefficient of species α in phase k and $\kappa_{\alpha,k}^{\text{eff}}$ is the electrical conductivity for species α. These terms, as well as Υ_k^α, are defined as

$$\frac{1 - \langle x_k^\alpha \rangle^*}{D_{\alpha,k}^{\text{eff}}} = \sum_{\beta \neq \alpha} \frac{\langle x_k^\beta \rangle^*}{D_{\alpha-\beta,k}^{\text{eff}}} + \frac{1}{D_{\alpha-s,k}^{\text{eff}}}, \tag{33}$$

$$\kappa_{\alpha,k}^{\text{eff}} = \frac{(z_\alpha)^2 \langle c_k^\alpha \rangle^* \mathscr{F} D_{\alpha,k}^{\text{eff}}}{\mathscr{R} \langle T_k \rangle^* (1 - \langle x_k^\alpha \rangle^*)}, \tag{34}$$

$$\Upsilon_k^\alpha = 1 + \frac{\partial \ln \langle \gamma_k^\alpha \rangle^*}{\partial \ln \langle x_k^\alpha \rangle^*}. \tag{35}$$

Mathematically, the interfacial source terms in Eqs. (24)–(27) are expressed as

$$\Gamma_{\text{M},k} = -\sum_n \frac{1}{V_r} \int_{A_{kn}} \rho_k (\boldsymbol{u}_k - \boldsymbol{u}_{kn}) \cdot \boldsymbol{n}_{kn} \, \mathrm{d}A, \tag{36}$$

$$\Gamma_{\text{F},k} = -\sum_n \frac{1}{V_r} \int_{A_{kn}} \rho_k \boldsymbol{u}_k (\boldsymbol{u}_k - \boldsymbol{u}_{kn}) \cdot \boldsymbol{n}_{kn} \, \mathrm{d}A$$

$$- \sum_n \frac{1}{V_r} \int_{A_{kn}} \tilde{P}_k \boldsymbol{n}_{kn} \, \mathrm{d}A - \sum_n \frac{1}{V_r} \int_{A_{kn}} \boldsymbol{\tau}_k \cdot \boldsymbol{n}_{kn} \, \mathrm{d}A, \tag{37}$$

$$\Gamma_{\text{S},k}^\alpha = -\sum_n \frac{1}{V_r} \int_{A_{kn}} \rho_k \omega_k^\alpha (\boldsymbol{u}_k - \boldsymbol{u}_{kn}) \cdot \boldsymbol{n}_{kn} \, \mathrm{d}A, \tag{38}$$

$$\Gamma_{\text{E},k} = -\sum_n \frac{1}{V_r} \int_{A_{kn}} \rho_k H_k (\boldsymbol{u}_k - \boldsymbol{u}_{kn}) \cdot \boldsymbol{n}_{kn} \, \mathrm{d}A$$

$$- \sum_n \frac{1}{V_r} \int_{A_{kn}} \boldsymbol{q}_k \cdot \boldsymbol{n}_{kn} \, \mathrm{d}A, \tag{39}$$

where $\sum_n$ represents the summation over all adjacent n phases, A_{kn} the interfacial area of phases k and n, and $\boldsymbol{u}_{kn}$ the velocity of the interface of k and n within the representative volume. The pressure deviation, $\tilde{P}_k$, is given by [36]

$$\tilde{P}_k = P_k - \langle P_k \rangle^*. \tag{40}$$

Physically, $\Gamma_{\text{M},k}$ represents the mass entering phase k from all adjacent phases. The momentum transfer from the adjacent phases to phase k due to mass transfer, pressure, and viscous forces is represented by $\Gamma_{\text{F},k}$. Species transfer from other phases is expressed as $\Gamma_{\text{S},k}^\alpha$, while $\Gamma_{\text{E},k}$ is the interfacial energy transfer due to mass transfer and molecular conduction.

Eqs. (24) and (27) represent the conservation of mass, momentum, species, and energy in the gas, liquid and solid phases of the PEM fuel cell. In order to solve these equations, constitutive equations are required for several parameters. Some constitutive equations apply throughout the PEM fuel cell; these are equations relating the temperatures of the fluid phases, the concentration of water in the gas phase, and the interfacial source term between the fluid and solid phases in the conservation of momentum equation. Local thermal equilibrium is assumed between the gas and liquid phases; therefore, the temperatures are equal:

$$\langle T_l \rangle^* = \langle T_g \rangle^*. \tag{41}$$

Also, if the liquid phase is present, the partial pressure of water within the gas phase is equal to the vapor pressure in the water; therefore,

$$\langle x_g^{\text{H}_2\text{O}} \rangle^* = \frac{P_{\text{sat}}^{\text{H}_2\text{O}}}{\langle P_g \rangle^*}. \tag{42}$$

The momentum interfacial source term between the fluid and solid phases can be modeled with the Darcy-Forchheimer terms [42]:

$$\Gamma_{\text{M},k} = -\frac{(\epsilon_k)^2 \mu_k}{K k_{rk}} \langle \boldsymbol{u}_k \rangle^* - \frac{\langle \rho_k \rangle^* (\epsilon_k)^3 F}{\sqrt{K k_{rk}}} |\langle \boldsymbol{u}_k \rangle^*| \langle \boldsymbol{u}_k \rangle^*, \tag{43}$$

where K is the absolute permeability of the porous media, k_{rk} the relative permeability, and F the Forchheimer term. If no solid phase exists, then $K = \infty$ and $F = 0$. The absolute permeability and the Forchheimer term depend on the structure of the porous media, while the relative permeabilities are functions of ϵ_k. The F term is not expected to be significant in the polymer electrolyte, due to the low fluid velocities. However, it will be significant in the electrode backing layer in the region adjacent to the gas flow channels [42].

The form for most of the constitutive equations required for closure of Eqs. (24)–(27) are location-specific, with different forms being required in the polymer electrolyte layer, electrode backing layer, gas flow channel, and catalyst layer. Specifically, expressions for the

- Volume fraction;
- Body forces;
- Pressure difference between the phases;
- Reaction kinetics and corresponding interfacial source term for the conservation of species equation; and
- Interfacial source term for the energy equation

are required. However, not all of the above-mentioned parameters are required in each layer. The body force is only significant in the polymer electrolyte and catalyst layers, while only a relationship between the gas and liquid pressures is required within the gas flow channels. The relevant constitutive equations for each layer are examined in the following sections.

4.1. Formulation for the polymer electrolyte

The gas, water, and proton transport properties of the polymer electrolyte are functions of the membrane water content ($\mathscr{L}$), which is defined as

$$\mathscr{L} = \frac{\text{moles of liquid water}}{\text{moles of } SO_3H}. \tag{44}$$

As the electrolyte absorbs more water, the value of $\mathscr{L}$ increases. The transport of water and ions in the electrolyte can only occur if the water content is above a minimum level ($\mathscr{L}_{min}$) [5]. Hence, the percolation model should be applied to the effective diffusion coefficients within the electrolyte [9], whereby $D_{\alpha-\beta,\ell}^{eff} = 0$ if $\mathscr{L} < \mathscr{L}_{min}$.

The volume fraction of the membrane available for water and proton transport becomes [9]

$$\epsilon_l = \frac{\mathscr{L}}{(\hat{V}_s/\hat{V}_{H_2O}) + \mathscr{L}}, \tag{45}$$

where $\hat{V}_s$ is the partial molar volume of the polymer and $\hat{V}_{H_2O}$ the partial molar volume of liquid water. The permeability of the electrolyte to both gas and liquid increases as the water content increases [31]; this implies that the relative permeability and the volume fraction of the gas phase are proportional to the membrane water content:

$$k_{rk} = \zeta_k \mathscr{L}, \qquad \epsilon_g = \zeta_\epsilon \mathscr{L},$$

where the constant of proportionality is expressed as ζ. The percolation model should also be applied to the relative permeability of the liquid water; hence, $k_{r\ell} = 0$ if $\mathscr{L} < \mathscr{L}_{min}$.

An electrical potential gradient exists within the polymer electrolyte, and this gradient exerts a body force on the water/hydronium ion mixture. Therefore, within the liquid phase of the polymer electrolyte, the body force is defined as [7]

$$\langle \boldsymbol{b}_l \rangle^* = -\langle c_l^{H_3O^+} \rangle^* \mathscr{F} \nabla \langle \Phi_e \rangle^*, \tag{46}$$

where $c_l^{H_3O^+}$ is the molar concentration of H_3O^+ in the liquid phase and Φ_e the potential in the polymer electrolyte. The body force of Eq. (46) is responsible for the electro-osmotic drag effect in the polymer electrolyte.

The relationship between the pressures in the gas and liquid phases are unknown; due to the small geometry of the pores, direct measurement is impossible. However, since the area in which the gas transport occurs is flexible, it will be assumed that the pressures in the gas and liquid phases are equal. Hence

$$\langle P_g \rangle^* = \langle P_l \rangle^*. \tag{47}$$

The concentrations of H_3O^+ and liquid water are related through the acid–base equilibrium reaction occurring within the electrolyte pores [9]:

$$SO_3H + H_2O \rightleftharpoons H_3O^+ + SO_3^-. \tag{48}$$
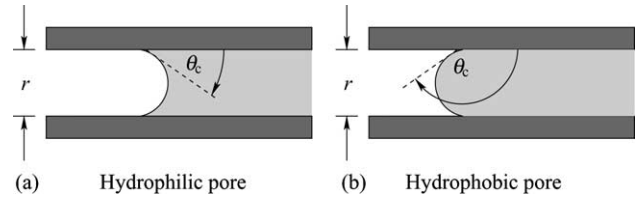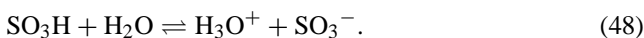

Fig. 4. Cylindrical pore having (a) hydrophilic and (b) hydrophobic characteristics.

Using a mass balance, the mole fractions of hydronium and liquid water in the pores of the electrolyte become a function of the membrane hydration [9]:

$$\langle x_1^{H_3O^+} \rangle^* = \frac{1}{\mathscr{L}} \left[\frac{(1 + \mathscr{L}) - \sqrt{(1 + \mathscr{L}_e)^2 - 4\mathscr{L}(1 - \mathbb{K}_e^{-1})}}{2(1 - \mathbb{K}_e^{-1})} \right], \tag{49}$$

where $\mathbb{K}_e$ is the equilibrium constant for reaction (48).

The small pore size makes the assumption of local thermodynamic equilibrium between the solid and fluid phases within the polymer electrolyte layer reasonable. Therefore, within the polymer electrolyte layer,

$$\langle T_g \rangle^* = \langle T_l \rangle^* = \langle T_s \rangle^*. \tag{50}$$

4.2. Formulation for the electrode backing layer

In the electrode backing layer, the volume fraction of the solid phase is a design parameter. Therefore, it is convenient to define the saturation of the gas or liquid phase as

$$s_k = \frac{\epsilon_k}{\phi}, \tag{51}$$

where the void fraction (ϕ) is the volume available to the fluid phases, with $\phi = 1 - \epsilon_s$.

The pressures in the gas and liquid phases are related with the capillary pressure:

$$P_c = \langle P_g \rangle^* - \langle P_l \rangle^*. \tag{52}$$

Both the relative permeability (k_{rk}) and the capillary pressure are a function of the liquid saturation in the porous media. In a cylindrical pore, the difference between the gas and liquid pressure is a function of the surface tension, contact angle, and pore radius [43]:

$$P_c = \frac{2\sigma \cos \theta_c}{r}, \tag{53}$$

where σ is the surface tension between the gas and liquid phases, θ_c is the contact angle, and r is the pore radius. If the pore material is hydrophilic, the contact angle is less than $90°$ and P_c is positive; hydrophobic materials have a negative P_c and the water contact angle is greater than $90°$, as illustrated in Fig. 4.

A porous media can be considered to be composed of a large distribution of pores with different dimensions, with the water content of each pore depending on the applied capillary pressure. The variation of capillary pressure with water content in porous media is illustrated in Fig. 5. For hydrophilic porous media, the capillary pressure is always positive, as shown in Fig. 5(a), while Fig. 5(b) illustrates that hydrophobic porous media are characterized by negative capillary pressures. Mixed-wettability porous media, shown in Fig. 5(c), can exhibit both positive and negative capillary pressures [44].

All three capillary pressure curves have two similar features. The first is the existence of hysteresis, with different curves being produced if water is entering (wetting) or leaving (drying) the porous media; thus the capillary pressure depends on both liquid saturation and history. The hysteresis is due to the difference in contact angle for advancing and receding water [45].

The second common feature between the two capillary pressure curves is that the capillary pressure asymptotically approaches infinity at a finite, minimum value of saturation, and approaches negative infinity for a maximum value of water saturation. This can be interpreted as there being a residual saturation of water, s_{lr}, and a residual saturation of gas, s_{gr}, in the porous media. The residual saturation represents the saturation at which the fluid loses the capability to move as a bulk phase in response to a hydraulic gradient, resulting in the transport of the residual fluid being dominated by advective–diffusive transport as a dispersed phase in the fluid with the larger volume fraction [46].

Attempts have been made to correlate capillary pressure curves, with a comprehensive representation being [46]

$$P_{NW} - P_W = 2\mathcal{Z}\sigma \cos(\theta_{cW}) \sqrt{\frac{\epsilon}{K}} \mathcal{L}(s_W^{eff}), \tag{54}$$

where P_{NW} and P_W are the pressures of the non-wetting and wetting fluids, respectively, $\mathcal{Z}$ is a correction factor to account for the change in contact angle due to roughness, θ_{cW} is the intrinsic contact angle of the wetting fluid to the solid, and $\mathcal{L}(s_W^{eff})$ is a function of the effective saturation of the wetting fluid. The effective saturation is defined as

$$s_W^{eff} = \frac{s_W - s_{Wr}}{1 - s_{NWr} - s_{Wr}}, \tag{55}$$

where s_{NWr} and s_{Wr} are the residual saturations of the non-wetting and wetting fluids, respectively. Therefore, if one capillary pressure curve is available, it can be applied to different porous media, using corrections for the porosity, permeability and roughness. However, the function $\mathcal{L}$ is not fully universal, and depends on several other parameters, such as pore structure.

Predictive models for the relative permeability were developed from conceptual models of flow in capillary tubes combined with models of pore-size distribution [47]. The common conceptual models are the Burdine and Mualem functions. In addition to the conceptual models, several porous media modeling studies have successfully used a simple power law relationship for the relative permeability [40]:

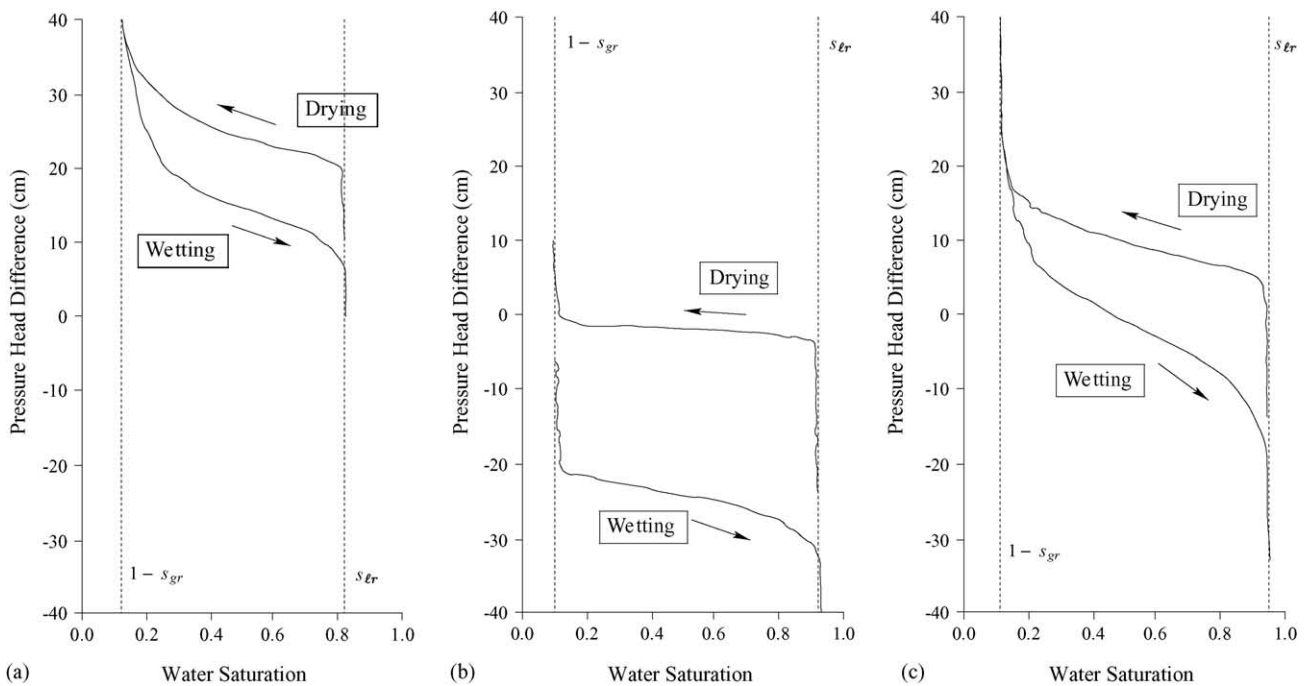$$k_{rg} = (s_g^{eff})^n, \qquad k_{rl} = (s_l^{eff})^n. \tag{56}$$

Fig. 5. Variation of capillary pressure with liquid saturation for (a) hydrophilic, (b) hydrophobic, and (c) mixed-wettability porous media [44]. The pressure head difference is equal to $P_c/(\rho_{lg})$, where P_c is the capillary pressure and g is the acceleration due to gravity.

The temperature of the solid and fluid phases may be unequal; thus, an expression for the interfacial heat transfer between the solid and fluid phases is required. One method is to use a convective heat transfer coefficient [48]:

$$\Gamma_{E,k} = h_{ks}\hat{A}_{ks}(\langle T_s\rangle^* - \langle T_k\rangle^*), \tag{57}$$

where h_{ks} is the convection coefficient and $\hat{A}_{ks}$ is the interfacial area per unit volume. Correlations for the convection coefficient are available from the published literature [40].

4.3. Formulation for the gas flow channel

No solid phase exists in the gas flow channels; hence, no interfacial source terms are required. Since the water is assumed to be in suspended droplet form, the relationship between the pressures can be expressed as

$$\langle P_g\rangle^* - \langle P_l\rangle^* = -\frac{2\sigma}{r}, \tag{58}$$

where σ is the surface tension and r is the characteristic radius of the droplet.

4.4. Formulation for the catalyst layer

The catalyst layer is a porous media, similar to the electrode backing layer; however, the structure is more complicated due to the fact that polymer electrolyte exists within the pore region. Fig. 6 shows that the gas and liquid phases are contained within two structures: the void region of the catalyst layer and the polymer electrolyte. Therefore, five sets of conservation equations are applied in the catalyst layer, with

1. $k = g$ referring to the gas phase in the void region;
2. $k = l$ referring to the liquid phase in the void region;
3. $k = g$, e referring to the gas phase within the polymer electrolyte;
4. $k = l$, e referring to the liquid phase within the polymer electrolyte;
5. $k = s$ referring to the carbon support and catalyst.

The conservation equations for $k = g$, l, and s are similar to the corresponding equations in the electrode backing layer, while the $k = g$, e and l, e cases are similar to the equations in the polymer electrolyte layer. The volume fractions can be expressed as

$$\epsilon_g = \phi s_g, \quad \epsilon_l = \phi s_l, \quad \epsilon_{g,e} = \phi s_e \epsilon_g^e, \quad \epsilon_{l,e} = \phi s_e \epsilon_l^e,$$

where $\phi = 1 - \epsilon_s$ and ϵ_g^e and ϵ_l^e are the volume fractions of the electrolyte that contain gas and liquid phase, respectively. The pressure relationship between the gas and liquid phases in the void region are the same as in the electrode backing layer, while the pressure in the polymer electrolyte is considered to be the result of the gas and liquid phase pressures:

$$\langle P_{g,e}\rangle^* = \langle P_{l,e}\rangle^* = \frac{s_g}{1 - s_e}\langle P_g\rangle^* + \frac{s_l}{1 - s_e}\langle P_l\rangle^*. \tag{59}$$

The water content of the polymer electrolyte is determined by the water content of the gas and liquid phases within the void region of the catalyst layer:

$$\mathscr{L} = \frac{s_g\mathscr{L}_g + s_l\mathscr{L}_l}{1 - s_e}, \tag{60}$$

where $\mathscr{L}_g$ and $\mathscr{L}_l$ are the hydrations when the membrane is in contact with a gas or liquid phase, respectively. The value of
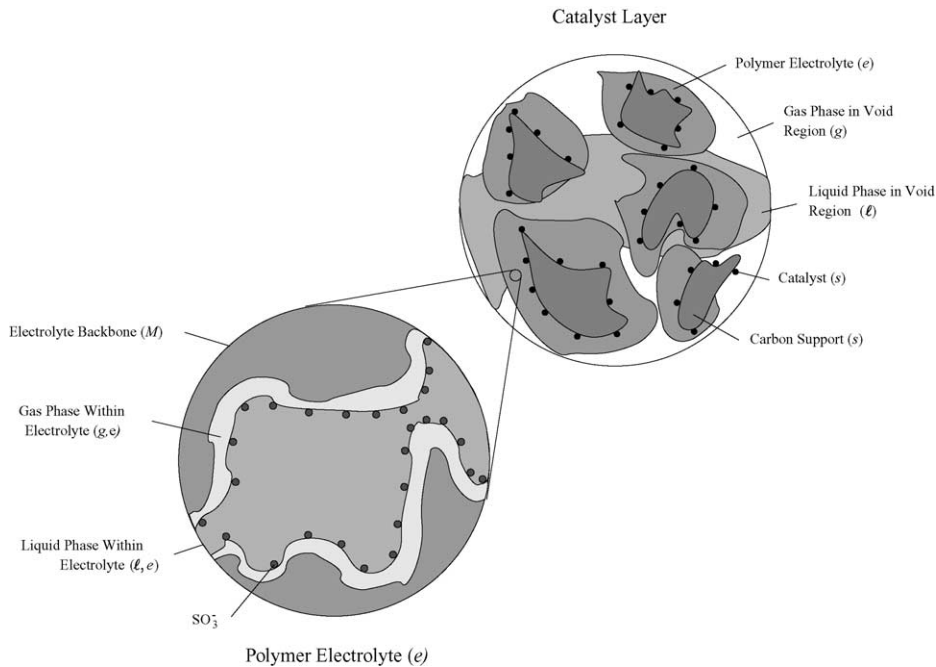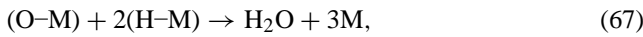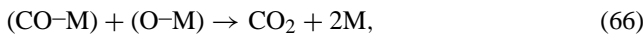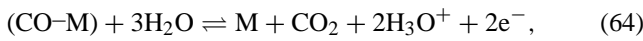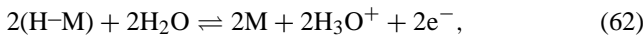

Fig. 6. The structure of the catalyst layer.

$\mathscr{L}_1$ can be considered as a function of temperature only [49], but the value of $\mathscr{L}_g$ is a function of both temperature and the concentration of water vapor in the gas phase. The value of $\mathscr{L}_g$ can be found using a Flory-Huggins model [50].

Electro-chemical and heterogeneous reactions occur on the interface between the polymer electrolyte and the solid phases in the catalyst layers. The interfacial source terms in the conservation of species equation represent the rate of production of each species; this rate of production is determined by the reaction kinetics. In the anode catalyst layer, the following reactions are considered [6]:

1. Hydrogen adsorption, desorption and electro-oxidation;
2. Carbon monoxide adsorption, desorption and electro-oxidation;
3. Heterogeneous oxidation of carbon monoxide by oxygen;
4. Heterogeneous oxidation of hydrogen by oxygen.

Hence, the reactions can be expressed as

$$H_2 + 2M \rightleftharpoons 2(H\text{–}M), \tag{61}$$

$$2(H\text{–}M) + 2H_2O \rightleftharpoons 2M + 2H_3O^+ + 2e^-, \tag{62}$$

$$CO + M \rightleftharpoons (CO\text{–}M), \tag{63}$$

$$(CO\text{–}M) + 3H_2O \rightleftharpoons M + CO_2 + 2H_3O^+ + 2e^-, \tag{64}$$

$$O_2 + 2M \rightleftharpoons 2(O\text{–}M), \tag{65}$$

$$(CO\text{–}M) + (O\text{–}M) \rightarrow CO_2 + 2M, \tag{66}$$

$$(O\text{–}M) + 2(H\text{–}M) \rightarrow H_2O + 3M, \tag{67}$$

where reactions (61) and (62) represent the adsorption and electro-oxidation of hydrogen, assumed to follow Langmuir and Butler–Volmer kinetics, respectively; reactions (63) and (64) are the adsorption and electro-oxidation of carbon monoxide, assumed to follow Temkin and Butler–Volmer kinetics, respectively; and reactions (65)–(67) denote the heterogeneous oxidation of hydrogen and carbon monoxide, assumed to follow Langmuir–Hinshelwood kinetics. The reaction rates, in units of mole m^{-2} s^{-1}, are

$$\mathcal{R}_{a,ads}^{H} = k_{ads}^{H}(c_{g,e}^{H_2}(\theta_s^{M})^2 - b_{ads}^{H}(\theta_s^{H})^2), \tag{68}$$

$$\mathcal{R}_{a,ox}^{H} = \frac{J_0^{H}}{\mathscr{F}} \left\{ \left[\frac{\theta_s^{H}}{\bar{\theta}_s^{H}} \right] \right.$$
$$\left. \times \exp\left(\frac{\eta_a}{B_a^{H}} \right) - \left[\frac{\theta_s^{M}}{\bar{\theta}_s^{M}} \right] \left[\frac{c_{1,e}^{H_3O^+}}{\bar{c}_{1,e}^{H_3O^+}} \right] \exp\left(-\frac{\eta_a}{B_a^{H}} \right) \right\}, \tag{69}$$

$$\mathcal{R}_{a,ads}^{CO} = k_{ads}^{CO} \left\{ c_{g,e}^{CO}\theta_s^{M} \exp\left(-\frac{\beta r \theta_s^{CO}}{\mathscr{R}T_i} \right) - b_{ads}^{CO}\theta_s^{CO} \right.$$
$$\left. \times \exp\left(\frac{[1-\beta]r\theta_s^{CO}}{\mathscr{R}T_i} \right) \right\}, \tag{70}$$

$$\mathcal{R}_{a,ox}^{CO} = \frac{J_0^{CO}}{2\mathscr{F}} \left\{ \left[\frac{\theta_s^{CO}}{\bar{\theta}_s^{CO}} \right] \left[\frac{c_{1,e}^{H_2O}}{\bar{c}_{1,e}^{H_2O}} \right]^2 \exp\left(\frac{\eta_a}{B_a^{CO}} \right) \right.$$
$$\left. - \left[\frac{\theta_s^{M}}{\bar{\theta}_s^{M}} \right] \left[\frac{c_{g,e}^{CO_2}}{\bar{c}_{g,e}^{CO_2}} \right] \left[\frac{c_{1,e}^{H_3O^+}}{\bar{c}_{1,e}^{H_3O^+}} \right]^3 \exp\left(-\frac{\eta_a}{B_a^{CO}} \right) \right\}, \tag{71}$$

$$\mathcal{R}_{a,ads}^{O} = k_{ads}^{O}\{c_{g,e}^{O_2}(\theta_s^{M})^2 - b_{ads}^{O}(\theta_s^{O})^2\}, \tag{72}$$

$$\mathcal{R}_{a,ox}^{H\text{–}O} = k_{ox}^{H\text{–}O}\{\theta_s^{O}(\theta_s^{H})^2 - b_{ox}^{H\text{–}O}c_{1,e}^{H_2O}(\theta_s^{M})^3\}, \tag{73}$$

$$\mathcal{R}_{a,ox}^{CO\text{–}O} = k_{ox}^{CO\text{–}O}\{\theta_s^{O}\theta_s^{CO} - b_{ox}^{CO\text{–}O}c_{g,e}^{CO_2}(\theta_s^{M})^2\}, \tag{74}$$

where k_i^{α} denotes the forward rate reaction constant, b_i^{α} denotes the ratio of backward to forward reaction rate constant, and J_0^{α} is the exchange current density. The fraction of the platinum reaction sites in the solid phase covered by species α is denoted by θ_s^{α}, with $\theta_s^{M} = 1 - \theta_s^{H} - \theta_s^{CO} - \theta_s^{O}$ representing the fraction of free reaction sites. The interface temperature is represented by T_i and the concentrations are assumed to be equivalent to the volume-averaged concentrations. An overbar over the concentration or coverage, "$^-$", represents the value at equilibrium, or when the reaction rates are zero.

The overpotential of the anode catalyst layer is denoted as η_a and is defined as [32]

$$\eta_a = \Phi_s - \Phi_e - U_a', \tag{75}$$

where the value of U_a' is taken as zero. In the carbon monoxide adsorption/desorption reaction rate, Eq. (70), β is a symmetry factor that has a value between zero and one, and r is an interaction parameter that represents the effect of lateral-interaction on the adsorption/desorption process [51]. In Eqs. (69) and (71), B_a^{α} is the Tafel slope for species α; the Tafel slopes for the forward and backward directions are considered equivalent, with

$$B_a^{H} = B_a^{CO} = \frac{2\mathscr{R}T_i}{\mathscr{F}}. \tag{76}$$

The production of reaction intermediates (θ_s^{H}, θ_s^{CO}, and θ_s^{O}) are assumed to be in steady state; thus,

$$\dot{\mathscr{P}}_a^{\theta_s^{H}} = 2\mathcal{R}_{a,ads}^{H} - \mathcal{R}_{a,ox}^{H} - 2\mathcal{R}_{a,ox}^{H\text{–}O} = 0, \tag{77}$$

$$\dot{\mathscr{P}}_a^{\theta_s^{CO}} = \mathcal{R}_{a,ads}^{CO} - \mathcal{R}_{a,ox}^{CO} - \mathcal{R}_{a,ox}^{CO\text{–}O} = 0, \tag{78}$$

$$\dot{\mathscr{P}}_a^{\theta_s^{O}} = 2\mathcal{R}_{a,ads}^{O} - \mathcal{R}_{a,ox}^{H\text{–}O} - \mathcal{R}_{a,ox}^{CO\text{–}O} = 0. \tag{79}$$

Using Eqs. (77)–(79), the production of the reactants and products can be expressed in terms of $\mathcal{R}_{a,ox}^{H}$, $\mathcal{R}_{a,ox}^{CO}$, $\mathcal{R}_{a,ox}^{H\text{–}O}$ and $\mathcal{R}_{a,ox}^{CO\text{–}O}$:

$$\dot{\mathscr{P}}_a^{H_2} = -\frac{1}{2}\mathcal{R}_{a,ox}^{H} - \mathcal{R}_{a,ox}^{H\text{–}O},$$

$$\dot{\mathscr{P}}_a^{CO} = -\mathcal{R}_{a,ox}^{CO} - \mathcal{R}_{a,ox}^{CO-O},$$

$$\dot{\mathscr{P}}_a^{O_2} = -\frac{1}{2}\mathcal{R}_{a,ox}^{H-O} - \frac{1}{2}\mathcal{R}_{a,ox}^{CO-O},$$

$$\dot{\mathscr{P}}_a^{e^-} = \mathcal{R}_{a,ox}^{H} + 2\mathcal{R}_{a,ox}^{CO}, \quad \dot{\mathscr{P}}_a^{H_3O^+} = \mathcal{R}_{a,ox}^{H} + 2\mathcal{R}_{a,ox}^{CO},$$

$$\dot{\mathscr{P}}_a^{H_2O} = -\mathcal{R}_{a,ox}^{H} - 3\mathcal{R}_{a,ox}^{CO} + \mathcal{R}_{a,ox}^{H-O},$$

$$\dot{\mathscr{P}}_a^{CO_2} = \mathcal{R}_{a,ox}^{CO} + \mathcal{R}_{a,ox}^{CO-O}.$$

The major reaction occurring in the cathode catalyst layer is oxygen reduction:

$$O_2 + 4H_3O^+ + 4e^- \rightleftharpoons 6H_2O. \tag{80}$$
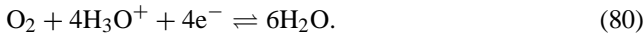
The rate of reaction is governed by Volmer/Erdey-Gruz kinetics [52]:

$$\mathcal{R}_{c,red}^{O_2} = \frac{J_0^{O_2}}{4\mathscr{F}}\left\{\left[\frac{c_{g,e}^{O_2}}{\bar{c}_{g,e}^{O_2}}\right]\left[\frac{c_{1,e}^{H_3O^+}}{\bar{c}_{1,e}^{H_3O^+}}\right]^4 \exp\left(-\frac{\eta_c}{B_c^{O_2}}\right)\right.$$

$$\left. - \left[\frac{c_{1,e}^{H_2O}}{\bar{c}_{1,e}^{H_2O}}\right]^6 \exp\left(\frac{\eta_c}{B_c^{O_2}}\right)\right\}, \tag{81}$$

where $J_0^{O_2}$ is the exchange current density for oxygen reduction. The Tafel slope is denoted by $B_c^{O_2}$ and is given by

$$B_c^{O_2} = \frac{\mathscr{R}T}{\mathscr{F}}. \tag{82}$$

Eq. (82) results in a Tafel slope of 68 mV/decade at a temperature of 70 °C, which agrees with the experimental value of 70 mV/decade from Parthasarathy et al. [53].

Gases can dissolve into the polymer electrolyte and be transported between the anode and cathode; however transport of gases in the polymer electrolyte is slow. Since CO is present in only a ppm amount, it is unlikely that a significant amount could be transported across the polymer electrolyte membrane layer and react in the cathode catalyst layer. However, cross-over of hydrogen could be possible and as a result, the heterogeneous oxidation of hydrogen by oxygen is included in the cathode catalyst layer. The chemical reaction and reaction rate are represented in the same manner as in the anode catalyst layer; hence, the net production of each species in the cathode catalyst layer is

$$\dot{\mathscr{P}}_c^{O_2} = -\mathcal{R}_{c,red}^{O_2} - \frac{1}{2}\mathcal{R}_{c,ox}^{H-O}, \quad \dot{\mathscr{P}}_c^{H_2} = -\mathcal{R}_{c,ox}^{H-O},$$

$$\dot{\mathscr{P}}_c^{H_2O} = 6\mathcal{R}_{c,red}^{O_2} + \mathcal{R}_{c,ox}^{H-O},$$

$$\dot{\mathscr{P}}_c^{H_3O^+} = -4\mathcal{R}_{c,red}^{O_2}, \quad \dot{\mathscr{P}}_c^{e^-} = -4\mathcal{R}_{c,red}^{O_2}.$$

Using the reaction kinetics, the interfacial source term in the conservation of species equation is related to the $\dot{\mathscr{P}}^\alpha$ terms through

$$\Gamma_{S,k}^\alpha = \acute{A}_{\mathcal{R}}\hat{M}_\alpha \dot{\mathscr{P}}^\alpha, \tag{83}$$

$$\hat{\Gamma}_{S,k}^\alpha = \acute{A}_{\mathcal{R}}\dot{\mathscr{P}}^\alpha, \tag{84}$$

where $\acute{A}_{\mathcal{R}}$ is the reactive surface area per volume in the catalyst layer. The units of $\Gamma_{S,k}^\alpha$ are kg m^{-3} s^{-1}, while $\hat{\Gamma}_{S,k}^\alpha$ is in molar units of mole m^{-3} s^{-1}.

The reactions occurring within the catalyst layers are exothermic; thus, the heat of reaction, Q_{react}, is added to the conservation of energy in the solid phase [48]:

$$Q_{react} = \acute{A}_{\mathcal{R}}q_{react}, \tag{85}$$

$$q_{react} = -\sum_\alpha [\dot{\mathscr{P}}^\alpha \hat{H}_k^\alpha + \dot{\mathscr{P}}^\alpha \hat{H}_s^\alpha]$$

$$= q_{react,ir} + q_{react,rev} + q_{react,het}, \tag{86}$$

where $q_{react,ir}$ and $q_{react,rev}$ are the irreversible and reversible heat produced by the electro-chemical reactions. The heat produced by the heterogeneous chemical reactions is expressed as $q_{react,het}$. The irreversible heat production is a function of the overpotential:

$$q_{react,ir} = \begin{cases} \mathscr{F}\eta_a[\mathcal{R}_{a,ox}^{H} + 2\mathcal{R}_{a,ox}^{CO}] & \text{anode,} \\ -4\mathscr{F}\eta_c\mathcal{R}_{c,red}^{O_2} & \text{cathode.} \end{cases} \tag{87}$$

The reversible heat production is a function of the entropy change of the electro-chemical reactions:

$$q_{react,ir} = \begin{cases} -T_i[\mathcal{R}_{a,ox}^{H}\Delta\hat{S}_{R,ox}^{H} + \mathcal{R}_{a,ox}^{CO}\Delta\hat{S}_{R,ox}^{CO}] & \text{anode,} \\ -T_i\mathcal{R}_{c,red}^{O_2}\Delta\hat{S}_{R,red}^{O_2} & \text{cathode.} \end{cases}$$
$$\tag{88}$$

The change in entropy of the reactions, $\Delta\hat{S}_R$, are

$$\Delta\hat{S}_{R,ox}^{H} = \hat{S}_{1,e}^{H_3O^+} + \hat{S}_s^{e^-} - \frac{1}{2}\hat{S}_{g,e}^{H_2} - \hat{S}_{1,e}^{H_2O}, \tag{89}$$

$$\Delta\hat{S}_{R,ox}^{CO} = \hat{S}_{g,e}^{CO_2} + 2\hat{S}_{1,e}^{H_3O^+} + 2\hat{S}_s^{e^-} - \hat{S}_{g,e}^{CO} - 3\hat{S}_{1,e}^{H_2O}, \tag{90}$$

$$\Delta\hat{S}_{R,red}^{O_2} = 6\hat{S}_{1,e}^{H_2O} - \hat{S}_{g,e}^{O_2} - 4\hat{S}_{1,e}^{H_3O^+} - 4\hat{S}_s^{e^-}. \tag{91}$$

Finally, the heat produced by the heterogeneous oxidation of hydrogen and carbon monoxide is expressed as

$$q_{react,het} = \begin{cases} -\mathcal{R}_{a,ox}^{H-O}\Delta\hat{H}_R^{H-O} - \mathcal{R}_{a,ox}^{CO-O}\Delta\hat{H}_R^{CO-O} & \text{anode,} \\ -\mathcal{R}_{c,ox}^{H-O}\Delta\hat{H}_R^{H-O} & \text{cathode,} \end{cases}$$
$$\tag{92}$$

where the enthalpy changes are

$$\Delta\hat{H}_R^{H-O} = \hat{H}_{1,e}^{H_2O} - \hat{H}_{g,e}^{H_2} - \frac{1}{2}\hat{H}_{g,e}^{O_2}, \tag{93}$$

$$\Delta\hat{H}_R^{CO-O} = \hat{H}_{g,e}^{CO_2} - \hat{H}_{g,e}^{CO} - \frac{1}{2}\hat{H}_{g,e}^{O_2}. \tag{94}$$

5. Final set of governing equations

The previous sections outlined the governing equations for the conservation of mass, momentum, species and energy

in the gas and liquid phases, as well as the conservation of species and energy in the solid phase. Because the gas and liquid phases can be non-continuous, the fluid phases are combined to form a pseudo-fluid, or mixture. Thus, the processes occurring within the PEM fuel cell can be described by two sets of equations, with one set applying to the pseudo-fluid and the other set applying to the solid phase. The pseudo-fluid equations apply from $Y_{\text{bp/fc}}^{\text{a}} \leq y \leq Y_{\text{bp/fc}}^{\text{c}}$, while the equations for the solid phase apply between $0 \leq y \leq Y_{\text{cl/e}}^{\text{a}}$ and $Y_{\text{cl/e}}^{\text{c}} \leq y \leq Y_{\text{L}}$.

The properties of the pseudo-fluid are defined as

$$\rho_{\text{m}} = s_{\text{g}}\langle\rho_{\text{g}}\rangle^* + s_{\text{l}}\langle\rho_{\text{l}}\rangle^* + s_{\text{e}}\epsilon_g^{\text{e}}\langle\rho_{\text{g,e}}\rangle^* + s_{\text{e}}\epsilon_{\text{l}}^{\text{e}}\langle\rho_{\text{l,e}}\rangle^*, \quad (95)$$

$$\rho_{\text{m}}\boldsymbol{u}_{\text{m}} = s_{\text{g}}\langle\rho_{\text{g}}\rangle^*\langle\boldsymbol{u}_{\text{g}}\rangle^* + s_{\text{l}}\langle\rho_{\text{l}}\rangle^*\langle\boldsymbol{u}_{\text{l}}\rangle^* + s_{\text{e}}\epsilon_g^{\text{e}}\langle\rho_{\text{g,e}}\rangle^*\langle\boldsymbol{u}_{\text{g,e}}\rangle^*$$
$$+ s_{\text{e}}\epsilon_{\text{l}}^{\text{e}}\langle\rho_{\text{l,e}}\rangle^*\langle\boldsymbol{u}_{\text{l,e}}\rangle^*, \quad (96)$$

$$P_{\text{m}} = s_{\text{g}}\langle P_{\text{g}}\rangle^* + s_{\text{l}}\langle P_{\text{l}}\rangle^* + s_{\text{e}}\epsilon_g^{\text{e}}\langle P_{\text{g,e}}\rangle^* + s_{\text{e}}\epsilon_{\text{l}}^{\text{e}}\langle P_{\text{l,e}}\rangle^*, \quad (97)$$

$$\rho_{\text{m}}\omega_{\text{m}}^{\alpha} = s_{\text{g}}\langle\rho_{\text{g}}\rangle^*\langle\omega_{\text{g}}^{\alpha}\rangle^* + s_{\text{l}}\langle\rho_{\text{l}}\rangle^*\langle\omega_{\text{l}}^{\alpha}\rangle^* + s_{\text{e}}\epsilon_g^{\text{e}}\langle\rho_{\text{g,e}}\rangle^*\langle\omega_{\text{g,e}}^{\alpha}\rangle^*$$
$$+ s_{\text{e}}\epsilon_{\text{l}}^{\text{e}}\langle\rho_{\text{l,e}}\rangle^*\langle\omega_{\text{l,e}}^{\alpha}\rangle^*, \quad (98)$$

$$\rho_{\text{m}}H_{\text{m}} = s_{\text{g}}\langle\rho_{\text{g}}\rangle^*\langle H_{\text{g}}\rangle^* + s_{\text{l}}\langle\rho_{\text{l}}\rangle^*\langle H_{\text{l}}\rangle^* + s_{\text{e}}\epsilon_g^{\text{e}}\langle\rho_{\text{g}}\rangle^*\langle H_{\text{g}}\rangle^*$$
$$+ s_e\epsilon_{\text{l}}^{\text{e}}\langle\rho_{\text{l}}\rangle^*\langle H_{\text{l}}\rangle^*, \quad (99)$$

where ρ_{m}, $\boldsymbol{u}_{\text{m}}$, P_{m}, $\omega_{\text{m}}^{\alpha}$ and H_{m} are the density, velocity, pressure, mass fraction and enthalpy of the mixture, respectively.

Using the definitions of the mixture properties, the conservation of mass, momentum, species, and energy in the pseudo-fluid can be expressed as

$$\frac{\partial}{\partial t}(\phi\rho_{\text{m}}) + \nabla\cdot(\phi\rho_{\text{m}}\boldsymbol{u}_{\text{m}}) = 0, \quad (100)$$

$$\frac{\partial}{\partial t}(\phi\rho_{\text{m}}\boldsymbol{u}_{\text{m}}) + \nabla\cdot(\phi\rho_{\text{m}}\boldsymbol{u}_{\text{m}}\boldsymbol{u}_{\text{m}})$$
$$= -\nabla(\phi P_{\text{m}}) + \phi\rho_{\text{m}}\boldsymbol{g} + \nabla\cdot(\phi\boldsymbol{\tau}_{\text{m}}) + \mathcal{S}_{\text{mom,m}}, \quad (101)$$

$$\frac{\partial}{\partial t}(\phi\rho_{\text{m}}\omega_{\text{m}}^{\alpha}) + \nabla\cdot(\phi\rho_{\text{m}}\omega_{\text{m}}^{\alpha}\boldsymbol{u}_{\text{m}})$$
$$= \nabla\cdot(\phi\rho_{\text{m}}D_{\alpha,\text{m}}^{\text{eff}}\nabla\omega_{\text{m}}^{\alpha}) + \nabla\cdot\left(\frac{\phi s_{\text{e}}\epsilon_k^{\text{e}}\hat{M}_{\alpha}\kappa_{\alpha,k,e}^{\text{eff}}}{z_{\alpha}\mathscr{F}}\nabla\Phi_{\text{m}}\right)$$
$$+ \mathcal{S}_{\text{species,m}}, \quad (102)$$

$$\frac{\partial}{\partial t}(\phi\rho_{\text{m}}H_{\text{m}}) + \nabla\cdot(\phi\rho_{\text{m}}H_{\text{m}}\boldsymbol{u}_{\text{m}})$$
$$= \nabla\cdot(\phi\lambda_{\text{m}}^{\text{eff}}\nabla T_{\text{m}}) + \mathcal{S}_{\text{energy,m}}, \quad (103)$$

where $\boldsymbol{\tau}_{\text{m}}$ is the viscous stress, $D_{\alpha,\text{m}}^{\text{eff}}$ is the effective diffusivity of species α, and $\lambda_{\text{m}}^{\text{eff}}$ is the thermal conductivity in the pseudo-fluid. In Eq. (102), the potential in the mixture (Φ_{m})

is equivalent to the potential in the liquid phase of the polymer electrolyte ($\langle\Phi_e\rangle^*$). The mixture viscous stress, diffusion coefficient, and thermal conductivity are given with

$$\boldsymbol{\tau}_{\text{m}} = \mu_{\text{m}}^{\text{eff}}[\nabla\boldsymbol{u}_{\text{m}} + (\nabla\boldsymbol{u}_{\text{m}})^{\dagger}], \quad (104)$$

$$\mu_{\text{m}}^{\text{eff}} = \sum_k s_k\mu_k^{\text{eff}} + s_{\text{e}}\epsilon_k^{\text{e}}\mu_k^{\text{eff}}, \quad (105)$$

$$D_{\alpha,\text{m}} = \sum_k s_k D_{\alpha,k}^{\text{eff}} + s_{\text{e}}\epsilon_k^{\text{e}}\Upsilon_{k,e}^{\alpha}D_{\alpha,k,e}^{\text{eff}}, \quad (106)$$

$$\lambda_{\text{m}}^{\text{eff}} = \sum_k s_k\lambda_k^{\text{eff}} + s_{\text{e}}\epsilon_k^{\text{e}}\lambda_{k,e}^{\text{eff}}, \quad (107)$$

where the summation is over the gas and liquid phases.

The source term in the momentum equation, $\mathcal{S}_{\text{mom,m}}$, has three components:

$$\mathcal{S}_{\text{mom,m}} = \mathcal{S}_{\text{mom,m}}^P + \mathcal{S}_{\text{mom,m}}^{\text{solid}} + \mathcal{S}_{\text{mom,m}}^{\text{rel}}, \quad (108)$$

$$\mathcal{S}_{\text{mom,m}}^P = \sum_k P_k\nabla(\phi s_k) + P_{k,e}\nabla(\phi s_{\text{e}}\epsilon_k^{\text{e}}), \quad (109)$$

$$\mathcal{S}_{\text{mom,m}}^{\text{solid}} = -\frac{\phi^2\mu_{\text{m}}^{\text{eff}}}{K_{\text{m}}}\boldsymbol{u}_{\text{m}} - \frac{\phi^3\rho_{\text{m}}F_{\text{m}}}{\sqrt{K_{\text{m}}}}|\boldsymbol{u}_{\text{m}}|\boldsymbol{u}_{\text{m}}$$
$$- \sum_k\left[\frac{(\epsilon_k)^2\mu_k}{Kk_{rk}}\boldsymbol{w}_k + \frac{(\epsilon_{k,e})^2\mu_{k,e}}{K_ek_{rk,e}}\boldsymbol{w}_{k,e}\right.$$
$$+ \frac{\langle\rho_k\rangle^*(\epsilon_k)^3F}{\sqrt{Kk_{rk}}}|\langle\boldsymbol{u}_k\rangle^*|\boldsymbol{w}_k + \frac{\langle\rho_{k,e}\rangle^*(\epsilon_{k,e})^3F_{\text{e}}}{\sqrt{K_ek_{rk,e}}}$$
$$\left. \times|\langle\boldsymbol{u}_{k,e}\rangle^*|\boldsymbol{w}_{k,e}\right] + \epsilon_{\text{l,e}}\boldsymbol{b}_{\text{l,e}}, \quad (110)$$

$$\mathcal{S}_{\text{mom,m}}^{\text{rel}} = \nabla\cdot\left\{\phi\sum_k[s_k\mu_k^{\text{eff}}(\nabla\boldsymbol{w}_k + (\nabla\boldsymbol{w}_k)^{\dagger})\right.$$
$$\left. + s_{\text{e}}\epsilon_k^{\text{e}}\mu_{k,e}^{\text{eff}}(\nabla\boldsymbol{w}_{k,e} + (\nabla\boldsymbol{w}_{k,e})^{\dagger})]\right\}$$
$$- \nabla\cdot\left\{\phi\sum_k[s_k\langle\rho_k\rangle^*\boldsymbol{w}_k\boldsymbol{w}_k\right.$$
$$\left. + s_{\text{e}}\epsilon_k^{\text{e}}\langle\rho_{k,e}\rangle^*\boldsymbol{w}_{k,e}\boldsymbol{w}_{k,e}]\right\}, \quad (111)$$

where $\mathcal{S}_{\text{mom,m}}^P$ represents momentum transfer due to interfacial pressure differences, $\mathcal{S}_{\text{mom,m}}^{\text{solid}}$ represents momentum transfer due to the solid surface and the electrical body force, and $\mathcal{S}_{\text{mom,m}}^{\text{rel}}$ represents momentum transfer due to relative phase motion. The permeability and Forchheimer term for the mixture are

$$\frac{\mu_{\text{m}}^{\text{eff}}}{K_{\text{m}}} = \sum_k\frac{(s_k)^2\mu_k}{Kk_{rk}} + \frac{(s_{\text{e}}\epsilon_k^{\text{e}})^2\mu_{k,e}}{K_ek_{rk,e}}, \quad (112)$$

$$\frac{\rho_\mathrm{m} F_\mathrm{m}}{\sqrt{K_\mathrm{m}}} = \sum_k \frac{\langle \rho_k \rangle^* (s_k)^3 F |\langle \boldsymbol{u}_k \rangle^*|}{\sqrt{K k_{rk}} |\boldsymbol{u}_\mathrm{m}|}$$

$$+ \frac{\langle \rho_{k,e} \rangle^* (s_\mathrm{e} \epsilon_k^\mathrm{e})^3 F_e |\langle \boldsymbol{u}_{k,e} \rangle^*|}{\sqrt{K_e k_{rk,e}} |\boldsymbol{u}_\mathrm{m}|}. \tag{113}$$

The relative phase velocities, $\boldsymbol{w}$, are defined as

$$\boldsymbol{w}_k = \langle \boldsymbol{u}_k \rangle^* - \boldsymbol{u}_\mathrm{m}, \tag{114}$$

$$\sum_k s_k \langle \rho_k \rangle^* \boldsymbol{w}_k + s_\mathrm{e} \epsilon_k^\mathrm{e} \langle \rho_{k,e} \rangle^* \boldsymbol{w}_{k,e} = 0. \tag{115}$$

The source term for the conservation of species equation, $\mathcal{S}_{\mathrm{species,m}}$, can also be decomposed into three components:

$$\mathcal{S}_{\mathrm{species,m}} = \mathcal{S}_{\mathrm{species,m}}^{\mathrm{react}} + \mathcal{S}_{\mathrm{species,m}}^{\mathrm{non\text{-}fick}} + \mathcal{S}_{\mathrm{species,m}}^{\mathrm{rel}}, \tag{116}$$

$$\mathcal{S}_{\mathrm{species,m}}^{\mathrm{react}} = \sum_k \Gamma_{S,k}^\alpha, \tag{117}$$

$$\mathcal{S}_{\mathrm{species,m}}^{\mathrm{non\text{-}fick}}$$
$$= -\sum_k \nabla \cdot [\phi \langle \rho_k \rangle^* s_k \Upsilon_k^\alpha D_{\alpha,k}^{\mathrm{eff}} \nabla(\omega_\mathrm{m}^\alpha - \langle \omega_k^\alpha \rangle^*)$$
$$+ \phi \langle \rho_{k,e} \rangle^* s_\mathrm{e} \epsilon_k^\mathrm{e} \Upsilon_{k,e}^\alpha D_{\alpha,k,e}^{\mathrm{eff}} \nabla(\omega_\mathrm{m}^\alpha - \langle \omega_{k,e}^\alpha \rangle^*)]$$
$$- \sum_k \nabla \cdot \left\{ \phi s_k \frac{\langle \omega_k^\alpha \rangle^* D_{\alpha,k}^{\mathrm{eff}}}{(1 - \langle x_k^\alpha \rangle^*)} \right.$$
$$\times \sum_{\beta \neq \alpha} \left[\frac{\langle \rho_k \rangle^* \Upsilon_k^\alpha \hat{M}_k}{\hat{M}_\beta} \nabla \langle \omega_k^\beta \rangle^* + \frac{\hat{M}_k \langle \mathcal{J}_k^\beta \rangle^*}{\hat{M}_\beta \mathscr{D}_{\alpha-\beta,k}^{\mathrm{eff}}} \right]$$
$$+ \phi s_k \langle \omega_k^\alpha \rangle^* \langle \rho_k \rangle^* \langle \boldsymbol{u}_k \rangle^* \left[\frac{D_{\alpha,k}^{\mathrm{eff}}}{(1 - \langle x_k^\alpha \rangle^*)} \sum_{\beta \neq \alpha} \frac{\langle x_k^\beta \rangle^*}{D_{\alpha-\beta,k}^{\mathrm{eff}}} - 1 \right]$$
$$+ \phi s_\mathrm{e} \epsilon_k^\mathrm{e} \frac{\langle \omega_{k,e}^\alpha \rangle^* D_{\alpha,k,e}^{\mathrm{eff}}}{(1 - \langle x_{k,e}^\alpha \rangle^*)}$$
$$\times \sum_{\beta \neq \alpha} \left[\frac{\langle \rho_{k,e} \rangle^* \Upsilon_{k,e}^\alpha \hat{M}_{k,e}}{\hat{M}_\beta} \nabla \langle \omega_{k,e}^\beta \rangle^* + \frac{\hat{M}_{k,e} \langle \mathcal{J}_{k,e}^\beta \rangle^*}{\hat{M}_\beta D_{\alpha-\beta,k,e}^{\mathrm{eff}}} \right]$$
$$+ \phi s_\mathrm{e} \epsilon_k^\mathrm{e} \langle \omega_{k,e}^\alpha \rangle^* \langle \rho_{k,e} \rangle^* \langle \boldsymbol{u}_{k,e} \rangle^*$$
$$\left. \times \left[\frac{D_{\alpha,k,e}^{\mathrm{eff}}}{(1 - \langle x_{k,e}^\alpha \rangle^*)} \sum_{\beta \neq \alpha} \frac{\langle x_{k,e}^\beta \rangle^*}{D_{\alpha-\beta,k,e}^{\mathrm{eff}}} - 1 \right] \right\}, \tag{118}$$

$$\mathcal{S}_{\mathrm{species,m}}^{\mathrm{rel}} = -\sum_k \nabla \cdot [\phi s_k \langle \omega_k^\alpha \rangle^* \langle \rho_k \rangle^* \boldsymbol{w}_k$$
$$+ \phi s_\mathrm{e} \epsilon_k^\mathrm{e} \langle \omega_{k,e}^\alpha \rangle^* \langle \rho_{k,e} \rangle^* \boldsymbol{w}_{k,e}], \tag{119}$$

where $\mathcal{S}_{\mathrm{species,m}}^{\mathrm{react}}$ represents the production or consumption of species α due to the electro-chemical reactions, $\mathcal{S}_{\mathrm{species,m}}^{\mathrm{non\text{-}fick}}$ are the non-Fickian terms of the Stefan–Maxwell equations, and $\mathcal{S}_{\mathrm{species,m}}^{\mathrm{rel}}$ is due to relative phase motion. While the source terms due to the non-Fickian terms and relative phase motion

are continuous, the production and consumption of reactants occurs only in the catalyst layers. Hence, $\mathcal{S}_{\mathrm{species,m}}^{\mathrm{react}}$ is only non-zero in the catalyst layers.

The source term in the conservation of energy equation, $\mathcal{S}_{\mathrm{energy,m}}$, can be considered as the sum of four terms:

$$\mathcal{S}_{\mathrm{energy,m}} = \mathcal{S}_{\mathrm{energy,m}}^{\mathrm{solid}} + \mathcal{S}_{\mathrm{energy,m}}^{\mathrm{H_3O^+}} + \mathcal{S}_{\mathrm{energy,m}}^{\mathrm{rel}}$$
$$+ \mathcal{S}_{\mathrm{energy,m}}^\mathrm{e}, \tag{120}$$

$$\mathcal{S}_{\mathrm{energy,m}}^{\mathrm{solid}} = h_\mathrm{m} \acute{A}_\mathrm{s} (\langle T_\mathrm{s} \rangle^* - T_\mathrm{m}), \tag{121}$$

$$\mathcal{S}_{\mathrm{energy,m}}^{\mathrm{H_3O^+}} = \phi s_\mathrm{e} \epsilon_1^\mathrm{e} \langle E_{1,e}^\pm \rangle^*, \tag{122}$$

$$\mathcal{S}_{\mathrm{energy,m}}^{\mathrm{rel}} = -\sum_k \nabla \cdot [\phi s_k \langle \rho_k \rangle^* \langle H_k \rangle^* \boldsymbol{w}_k$$
$$+ \phi s_\mathrm{e} \epsilon_k^\mathrm{e} \langle \rho_{k,e} \rangle^* \langle H_{k,e} \rangle^* \boldsymbol{w}_{k,e}], \tag{123}$$

$$\mathcal{S}_{\mathrm{energy,m}}^\mathrm{e} = -\frac{\partial}{\partial t} (\phi s_\mathrm{e} \epsilon_M^\mathrm{e} \rho_{M,e} C_{p,e} T_\mathrm{m}), \tag{124}$$

where $\mathcal{S}_{\mathrm{energy,m}}^{\mathrm{solid}}$ is the convective heat transfer between the solid and the mixture, $\mathcal{S}_{\mathrm{energy,m}}^{\mathrm{H_3O^+}}$ represents heat generation due to H_3O^+ migration, $\mathcal{S}_{\mathrm{energy,m}}^{\mathrm{rel}}$ is due to relative phase motion, and $\mathcal{S}_{\mathrm{energy,m}}^\mathrm{e}$ is the energy stored in the polymer backbone of the polymer electrolyte. The volume fraction, density, and specific heat of the polymer are ϵ_M^e, $\rho_{M,e}$, and $C_{p,e}$, respectively. The surface area of the solid phase is denoted by $\acute{A}_\mathrm{s}$.

The source terms in the mixture conservation equations are influenced by the relative phase velocities; expressions for $\boldsymbol{w}$ are required for closure. In order to develop expressions for the relative velocities, assumptions must be made on the nature of the flow in each component of the PEM fuel cell. The flow in the gas flow channels is considered to be homogeneous; thus, $\boldsymbol{w}_g = \boldsymbol{w}_l = 0$. In the electrode backing layers, the flow of liquid water is expected to be small. Hence, the relative velocity of the liquid phase can be determined by assuming that motion is governed by Darcy's law:

$$\boldsymbol{w}_l = -\frac{K k_{\mathrm{rl}}}{\phi s_l \mu_l} \nabla (\langle P_l \rangle^* - \langle \rho_l \rangle^* \boldsymbol{g}) - \boldsymbol{u}_\mathrm{m}. \tag{125}$$

The relative velocity of the gas phase can be determined with the relationship of Eq. (115).

In a similar manner, the relative velocity of the liquid phase in the polymer electrolyte layer can be determined by assuming that the flow can be described by the Schlögl equation:

$$\boldsymbol{w}_{l,e} = -\frac{K_e k_{\mathrm{rl,e}}}{\epsilon_1^\mathrm{e} \mu_{l,e}} \nabla (\langle P_{l,e} \rangle^* - \boldsymbol{b}_{l,e} - \langle \rho_l \rangle^* \boldsymbol{g}) - \boldsymbol{u}_\mathrm{m}. \tag{126}$$

The relative velocity of the gas phase within the polymer electrolyte can be calculated using Eq. (115).

The catalyst layer requires values for $\boldsymbol{w}_l$, $\boldsymbol{w}_{l,e}$ and $\boldsymbol{w}_{g,e}$, since $\boldsymbol{w}_g$ can be calculated with Eq. (115). The relative velocity of the liquid in the catalyst layer void space can be

found with Eq. (125), while $\boldsymbol{w}_{l,e}$ is given by Eq. (126). Assuming that the flow velocity of the gas phase within the polymer electrolyte is small, the relative velocity of the gas phase within the polymer electrolyte is

$$\boldsymbol{w}_{g,e} = -\frac{K_e k_{rg,e}}{\epsilon_g^e \mu_{g,e}} \nabla(\langle P_{g,e}\rangle^* - \langle\rho_{g,e}\rangle^* \boldsymbol{g}) - \boldsymbol{u}_m. \tag{127}$$

For the solid phase, only the conservation of species and energy are applicable. The flux of electrons is expressed in terms of current density, using Faraday's Law, and because electrons are the only mobile species in the solid phase, the Generalized Stefan–Maxwell equations reduce to Ohm's Law. Hence, the conservation of species and energy can be simplified to

$$0 = -\nabla \cdot (\epsilon_s \kappa_s^{\text{eff}} \nabla\langle\Phi_s\rangle^*) + \mathcal{S}_{\text{species},s}, \tag{128}$$

$$0 = \nabla \cdot (\epsilon_s \lambda_s^{\text{eff}} \nabla\langle T_s\rangle^*) + \mathcal{S}_{\text{energy},s}, \tag{129}$$

where $\mathcal{S}_{\text{species},s}$ and $\mathcal{S}_{\text{energy},s}$ are source terms. The source term in the conservation of species equation includes the consumption or production of electrons, while the source term for the conservation of energy equation includes the Joule heating term, convective heat transfer from the mixture, and the heat of the reaction:

$$\mathcal{S}_{\text{species},s} = \mathscr{F} \hat{\Gamma}_{S,s}^{e^-}, \tag{130}$$

$$\mathcal{S}_{\text{energy},s} = \epsilon_s \frac{|J_s|^2}{\kappa_s^{\text{eff}}} + h_m \acute{A}_s(T_m - \langle T_s\rangle^*) + Q_{\text{react}}. \tag{131}$$

The source term for the conservation of species equation is only non-zero in the catalyst layers; the heat of reaction is also non-zero in the catalyst layers.

Therefore, the processes occurring within a PEM fuel cell can be modeled with two sets of equations. The first set, Eqs. (100)–(103) describe the transport of mass, momentum, species, and energy within a mixture consisting of the gas and liquid phases. The second set, Eqs. (128) and (129), represent the migration of electrons and energy transport in the solid phase of the PEM fuel cell. If there are N uncharged species within the gas and liquid phases of the PEM fuel cell, the two sets of equations will sum to a total of $N + 5$ equations. These equations can be solved for the

- mixture velocity ($\boldsymbol{u}_m$) and pressure (P_m),
- $N - 1$ mixture mass fractions of the uncharged species (ω_s^α),
- potential in the solid phase ($\langle\Phi\rangle_s^*$) and electrolyte (Φ_m), and
- mixture enthalpy (H_m) and solid phase temperature ($\langle T_s\rangle^*$).

However, the source terms contained within the equation sets are functions of quantities within the individual phases, or phase quantities. As well, the mixture density is a function of the liquid saturation. Thus, the solution of the mixture conservation equations is iterative, and the mixture quantities must be converted into phase quantities at each itera-

tion. The first step in the conversion between the mixture and phase quantities is the determination of the liquid phase saturation (s_l). This is accomplished by setting $\alpha = H_2O$ in the definition of the mixture mass fraction, Eq. (98). If liquid water is present, the mass fraction of the water vapor can be determined with Eq. (42) and, if the electrolyte phase is also present, the mass fraction of liquid water within the electrolyte can be calculated by the acid-base equilibrium reaction. Since $s_g + s_l = 1$, Eq. (98) can be solved for s_l.

Once the liquid saturation is determined, the mixture density can be calculated with Eq. (95). Also, the pressure of the gas and liquid phases can be determined with the mixture pressure and the capillary pressure functions. With the individual phase pressures and Eqs. (125)–(127), the relative velocities of the gas and liquid phases can be calculated, along with the actual velocities of the gas and liquid phases. The mass fractions of each species within the gas and liquid phases can be determined with the mixture mass fractions and Eq. (98). The temperatures of the gas and liquid phases are assumed equal; hence, using equations of state and the definition of the mixture enthalpy, Eq. (99), the temperature of the gas and liquid phases can be found. Using the liquid saturation, the relative velocities of each phase, and the individual phase values of pressure, temperature, and species mass fractions, the source terms in the mixture and solid phase conservation equations can be evaluated. Therefore, new values of the mixture velocity, mixture pressure, mixture mass fractions, potentials, mixture enthalpy, and solid phase temperature can be evaluated.

After convergence of the iterative solution process, the mixture quantities can be converted into phase quantities, allowing for the display and analysis of the velocity, pressure, mass fractions, and temperatures within the individual phases. The cell voltage is specified as in input condition; hence, the cell performance can be quantified by the cell current, which is calculated using Eq. (7).

6. Conclusions

A mathematical, PEM fuel cell model was developed that described the conservation of mass, momentum, species and energy within the bipolar plates, gas flow channels, electrode backing, catalyst, and polymer electrolyte layers. The model consisted of two equation sets. The first equation set described the transport of mass, momentum, species, and energy within a mixture consisting of a gas and liquid phase. Electron migration and energy transport in the solid phase of the PEM fuel cell were considered with the second set of equations. The governing equations for the mixture and solid were derived using volume-averaging techniques.

The conservation equations for the mixture included source terms that represented fluid/solid interactions and effects due to relative phase motions. Thus, the source terms described the relevant phenomena that was significant in each

layer of the PEM fuel cell. Darcy-Forchheimer drag terms were included in order to account for the effect of the dispersed solid phase on the momentum of the fluid phases within the electrode backing, catalyst, and polymer electrolyte layers. Electro-osmotic drag in the electrolyte was incorporated with an electrical body force. Also, the consumption and production of species within the catalyst layers were included as a source term in the conservation of species equation. The equation set for the solid phase also included source terms, describing the production of electrons and the generation of heat due to the electro-chemical and heterogeneous reactions. Heat can also be transferred between the fluid and solid phases, through a source term representing convective heat transfer.

The equation sets for the fluid and solid phases are in a conservative form. Therefore, future work will involve applying methods from computational fluid dynamics (CFD) to solve the equation sets.

Acknowledgment

References

[1] D. Bernardi, M. Verbrugge, A mathematical model of the solid–polymer–electrolyte fuel cell, J. Electrochem. Soc. 139 (9) (1992) 2477–2491.

[2] F. Gloaguen, R. Durand, Simulations of PEFC cathodes: an effectiveness factor approach, J. Appl. Electrochem. 27 (9) (1997) 1029–1035.

[3] J. Baschuk, X. Li, Modelling of polymer electrolyte membrane fuel cells with variable degrees of water flooding, J. Power Sources 86 (1–2) (2000) 181–196.

[4] J.-T. Wang, R. Savinell, Simulation studies on the fuel electrode of a H_2–O_2, polymer electrolyte fuel cell, Electrochim. Acta 37 (15) (1992) 2737–2745.

[5] T. Springer, T. Rockward, T. Zawodzinski, S. Gottesfeld, Model for polymer electrolyte fuel cell operation on reformate feed: effects of CO, H_2 dilution, and high fuel utilization, J. Electrochem. Soc. 148 (1) (2001) A11–A23.

[6] J. Baschuk, X. Li, Mathematical model of a PEM fuel cell incorporating O_2 poisoning and O_2 (air) bleeding, Int. J. Global Energy Iss. 20 (3) (2003) 245–276.

[7] M. Verbrugge, R. Hill, Ion and solvent transport in ion-exchange membranes. I. A macrohomogeneous mathematical model, J. Electrochem. Soc. 137 (3) (1990) 886–899.

[8] T. Springer, T. Zawodzinski, S. Gottesfeld, Polymer electrolyte fuel cell model, J. Electrochem. Soc. 138 (8) (1991) 2334–2342.

[9] T. Thampan, S. Malhotra, H. Tang, R. Datta, Modeling of conductive transport in proton-exchange membranes for fuel cells, J. Electrochem. Soc. 147 (9) (2000) 3242–3250.

[10] V. Gurau, H. Liu, S. Kakac, Two-dimensional model for proton exchange membrane fuel cells, AIChE J. 44 (11) (1998) 2410–2422.

[11] S. Um, C. Wang, K. Chen, Computational fluid dynamics modeling of proton exchange membrane fuel cells, J. Electrochem. Soc. 147 (12) (2000) 4485–4493.

[12] N. Siegel, M. Ellis, D. Nelson, M. von Spakovsky, Single domain PEMFC model based on agglomerate catalyst geometry, J. Power Sources 115 (1) (2003) 81–89.

[13] T. Zhou, H. Liu, 3D model of proton exchange membrane fuel cells, Am. Soc. Mech. Eng. 366 (1) (2000) 43–49.

[14] S. Um, C. Wang, Three-dimensional analysis of transport and reaction in proton exchange membrane fuel cells, Am. Soc. Mech. Eng. 366 (1) (2000) 19–25.

[15] S. Shimpalee, S. Dutta, W. Lee, J.V. Zee, Effect of humidity on PEM fuel cell performance. Part II. Numerical simulation, Am. Soc. Mech. Eng. 364 (1) (1999) 367–374.

[16] T. Berning, D. Lu, N. Djilali, Three-dimensional computational analysis of transport phenomena in a PEM fuel cell, J. Power Sources 106 (1–2) (2002) 284–294.

[17] C. Wang, Z. Wang, Y. Pan, Two-phase phase transport in proton exchange membrane fuel cells, Am. Soc. Mech. Eng. 364 (1) (1999) 351–357.

[18] C. Wang, Multiphase flow and heat transfer in porous media, Adv. Heat Transfer 30 (1997) 93–196.

[19] W. He, J. Yi, T. Nguyen, Two-phase flow model of the cathode of PEM fuel cells using interdigitated flow fields, AIChE J. 46 (10) (2000) 2053–2064.

[20] S. Shimpalee, S. Dutta, J. Zee, Numerical prediction of local temperature and current density in a PEM fuel cell, Am. Soc. Mech. Eng. 366 (1) (2000) 1–9.

[21] L. You, H. Liu, A two-phase and multi-component model for the cathode of PEM fuel cells, Am. Soc. Mech. Eng. 369 (4) (2001) 325–334.

[22] Y. Ferng, C. Sun, A. Su, Numerical simulation of thermal–hydraulic characteristics in a proton exchange membrane fuel cell, Int. J. Energy Res. 27 (5) (2003) 495–511.

[23] J. Stockie, Modeling hydrophobicity in a porous fuel cell electrode. Presented at CFCD II, April 19–25, Banff International Research Station, Banff, Alberta, Canada, 2003.

[24] U. Pasaogullari, C. Wang, Liquid water transport in gas diffusion layer of polymer electrolyte fuel cells, J. Electrochem. Soc. 151 (3) (2004) A399–A406.

[25] U. Pasaogullari, C. Wang, Two-phase transport and the role of microporous layer in polymer electrolyte fuel cells, Electrochim. Acta 49 (25) (2004) 4359–4369.

[26] C. Marr, X. Li, An engineering model of proton exchange membrane fuel cell performance, ARI 50 (1998) 190–200.

[27] J. Baschuk, X. Li, Carbon monoxide poisoning of proton exchange membrane fuel cells, Int. J. Energy Res. 25 (8) (2001) 695–713.

[28] S. Gottesfeld, J. Pafford, A new approach to the problem of carbon monoxide poisoning in fuel cells operating at low temperatures, J. Electrochem. Soc. 135 (10) (1988) 2651–2652.

[29] D. Watkins, Research, development and demonstration of solid polymer fuel cell systems, in: L. Blomen, M. Mugerwa (Eds.), Fuel Cell Systems, Plenum Press, New York, 1993, pp. 493–530.

[30] T. Gierke, W. Hsu, The cluster-network model of ion clustering in perfluorosulfonated membranes, in: A. Eisenberg, H. Yeager (Eds.), Perfluorinated Ionomer Membranes, ACS Symposium Series, vol. 180, American Chemical Society, Washington, DC, 1982, pp. 283–307.

[31] Z. Ogumi, Z. Kuroe, Z. Takehara, Gas permeation in SPE method. II. Oxygen and hydrogen permeation through Nafion, J. Electrochem. Soc. 132 (11) (1985) 2601–2605.

[32] J. Newman, Electrochemical Systems, 2nd ed., Prentice-Hall, New Jersey, 1991.

[33] B. Hum, X. Li, Two-dimensional analysis of PEM fuel cells, J. Appl. Electrochem. 34 (2) (2004) 205–215.

[34] R. Bird, W. Stewart, E. Lightfoot, Transport Phenomena, 2nd ed., Wiley, New York, 2002.

[35] G. Castellan, Physical Chemistry, Addison-Wesley, Boston, 1983.

[36] S. Whitaker, Flow in porous media. I. A theoretical derivation of Darcy's law, Transport Porous Media 1 (1) (1986) 3–25.

[37] M. Ishii, Thermo-Fluid Dynamic Theory of Two-Phase Flow, Eyrolles, Paris, 1975.

[38] J. Slattery, Momentum, Energy, and Mass Transfer in Continua, 2nd ed., Robert E. Krieger Publishing Company, Huntington, 1981.

[39] C. Wang, W. Gu, B. Liaw, Micro-macroscopic coupled modeling of batteries and fuel cells. I. Model development, J. Electrochem. Soc. 145 (10–12) (1998) 3407–3417.

[40] M. Kaviany, Principles of Heat Transfer in Porous Media, 2nd ed., Springer, New York, 1995.

[41] E. Scattergood, E. Lightfoot, Diffusional interaction in an ion-exchange membrane, Trans. Faraday Soc. 64 (1968) 1135–1146.

[42] K. Vafai, S. Kim, Fluid mechanics of the interface region between a porous medium and a fluid layer: an exact solution, Int. J. Heat Fluid Flow 11 (3) (1990) 254–256.

[43] A. Adamson, Physical Chemistry of Surfaces, 5th ed., Wiley, New York, 1990.

[44] P. Ustohal, F. Stauffer, T. Dracos, Measurement and modeling of hydraulic characteristics of unsaturated porous media with mixed wettability, J. Contaminant Hydrol. 33 (1–2) (1998) 5–37.

[45] N. Morrow, Capillary pressure correlations for uniformly wetted porous media, J. Can. Petroleum Technol. 15 (4) (1976) 49–69.

[46] A. Demond, P. Roberts, Effect of interfacial forces on two-phase capillary pressure-saturation relationships, Water Resources Res. 27 (3) (1991) 423–437.

[47] J. Chen, J. Hopmans, M. Grismer, Parameter estimation of two-fluid capillary pressure-saturation and permeability functions, Adv. Water Resources 22 (5) (1999) 479–493.

[48] S. Chan, D. Hoang, Heat transfer and chemical reactions in exhaust system of a cold-start engine, Int. J. Heat Mass Transfer 42 (22) (1999) 4165–4183.

[49] J. Hinatsu, M. Mizuhata, H. Takenaka, Water uptake of perfluorosulfonic acid membranes from liquid water and water vapor, J. Electrochem. Soc. 141 (6) (1994) 1493–1498.

[50] P. Futerko, I. Hsing, Thermodynamics of water vapor uptake in perfluorosulfonic acid membranes, J. Electrochem. Soc. 146 (6) (1999) 2049–2053.

[51] E. Gileadi, E. Kirowa-Eisner, J. Penciner, Interfacial Electrochemistry: An Experimental Approach, Addison-Wesley, Boston, 1975.

[52] K. Vetter, Electrochemical Kinetics, Academic Press, New York, 1967.

[53] A. Parthasarathy, S. Srinivasan, A. Appleby, C. Martin, Temperature dependence of the electrode kinetics of oxygen reduction at the platinum/Nafion interface – a microelectrode investigation, J. Electrochem. Soc. 139 (9) (1992) 2530–2537.